Synthesis, Luminescence and Relaxometric Properties of Macrocyclic Lanthanide Complexes Appended with an Imidazothiadiazole, a Heterocyclic Bioactive Scaffold

Modou Ndiaye, Emma Caillet, Svetlana V. Eliseeva, Thibaut Masson, Luke Marchetti, Agnès Pallier, Jean-françois Morfin, Stéphane Petoud, Sylvain Routier, Frédéric Buron, et al.

RESEARCH ARTICLE

Synthesis, Luminescence and Relaxometric Properties of Macrocyclic Lanthanide Complexes Appended with an Imidazothiadiazole, a Heterocyclic Bioactive Scaffold

Modou Ndiaye,[a,b] Emma Caillet,[a,b] Svetlana V. Eliseeva,[a] Thibaut Masson,[b] Luke A. Marchetti,[a] Agnès Pallier,[a] Jean-François Morfin,[a] Stéphane Petoud,[a] Sylvain Routier,[b] Frédéric Buron, *[b] and Célia S. Bonnet*[a]

[a] M. Ndiaye, E. Caillet, Dr S. V. Eliseeva, Dr L. A. Marchetti, A. Pallier, Dr J-F. Morfin, Prof S. Petoud, Dr C.S. Bonnet
Centre de Biophysique Moléculaire
CNRS
Rue Charles Sadron, 45071 Orléans Cedex 2, France
E-mail: frederic.buron@univ-orleans.fr ; celia.bonnet@cnrs.fr

[b] M. Ndiaye, E. Caillet, Dr T. Masson, Prof. S. Routier, Dr. F. Buron
Institut de Chimie Organique et Analytique
UMR CNRS 7311, Université d'Orléans
Rue de Chartres, BP6759, 45067 Orléans, cedex 2, France

Supporting information for this article is given via a link at the end of the document

Abstract: The syntheses of two macrocycles containing original imidazothiadiazole heterocycles are presented. The protonation constants of the ligands have been determined by potentiometry and photophysical measurements. The photophysical properties of the corresponding Tb^{3+} complexes have been analyzed and the sensitization of the Tb^{3+} by the heterocyclic moiety demonstrated with modest quantum yields. The corresponding Gd^{3+} complexes are monohydrated and display higher relaxivities than GdDOTA, which could be explained by the larger size of these complexes. The different substitutions on the heterocycle does not affect strongly the protonation constants of the ligand, the quantum yield, water exchange rate and relaxation properties of the system.

Introduction

Magnetic Resonance Imaging (MRI) is one of the most efficient diagnostic modalities in clinical radiology and biomedical research. It is endowed with excellent time and spatial resolution, and unlimited tissue penetration. Today, Gd^{3+}-based complexes are routinely used as contrast agents for a better diagnosis. Their main effect is to decrease the longitudinal relaxation time (T_1) of surrounding water molecules.[1] Due to the intrinsic toxicity of free Gd^{3+} (and any Ln^{3+}), the complexes should display high thermodynamic stability and kinetic inertness.[2] The chelates used for stable Gd^{3+} complexation are macrocyclic or acyclic polyaminopolycarboxylate ligands, mostly based on DOTA (1,4,7,10-tetraazacyclododecane-1,4,7,10-tetraacetic acid) or DTPA (1,1,4,7,7-pentakis-(carboxymethyl)-1,4,7-triazaheptane) derivatives. It has been shown that macrocyclic complexes have superior kinetic inertness compared to acyclic complexes, and they are, therefore, preferred for clinical use.[3] GdDOTA, the gold-standard used routinely in clinics, has one water molecule directly coordinated to Gd^{3+} which can exchange with the bulk, making this complex an efficient contrast agent for MRI. Many derivatives of DOTA, particularly, DOTA-monoamide derivatives, have been studied over the years to improve the MRI efficacy (called relaxivity).[4] This has been mainly done by tuning the size of the system or the exchange rate of the water molecule directly coordinated to Gd^{3+}.[2] GdDOTA scaffolds have also been widely studied for the development of responsive or targeted contrast agents.[5] More recently the area of theranostics (combination of a therapeutic and diagnostic tool within the same platform) has emerged as a promising field in personalized medicine with the idea of reducing the number of agents administered to patient, and the possibility to simultaneously follow the efficacy of a treatment. Gd^{3+} complexes have been combined with different therapeutic tools to obtain theranostic agents.[5b, 6] For example, Gd^{3+}-based contrast agents have been used in combination with platinum complexes as anticancer agents,[7] porphyrins for photodynamic therapy.[8] They have also been used for Neutron Capture Therapy (NCT) by using the Gd properties[9] or in combination with boron.[10] Chemotherapy represents another class of widespread therapy using a drug or prodrug. Only few examples of Gd^{3+}-complexes appended with a drug have been described in the literature. GdDOTA monoamide complexes have been covalently linked to anticancer drugs such as colchicine,[11] chlorambucil,[12] benzothiazole,[13] camptothecin,[14] or anti-inflammatory conjugates.[15] Despite the fact that many drugs have a heterocyclic scaffold, very few examples have been described and none of them focus on the potential beneficial properties of the heterocyclic scaffold for diagnosis. Indeed, if the heterocycle is close to Gd^{3+}, the rotation of the whole complex will be slowed down, and/or the heteroatoms could potentially play a role in retaining water molecules by hydrogen bonding close to

Gd^{3+}, all that being beneficial to relaxation properties of the complex. Moreover, if Gd^{3+} is replaced by a luminescent Ln^{3+} such as Tb^{3+}, the heterocyclic scaffold could also play a role in sensitizing Ln^{3+} luminescence, which would render the system as a potential bimodal and theranostic probe, cumulating the advantages of MRI, optical imaging and therapy.

In the past decade, sulfur-containing [5,5] fused ring systems with a bridgehead nitrogen have received considerable attention in the drug discovery field due to their important role in the conception of biologically active products and in exploring uncovered regions of chemical space.[16] For example, these scaffolds have been reported in various therapeutic anticancer and antitubercular agents, and for cardiovascular treatments.[17]1 Among the isomers, imidazo[2,1-*b*][1,3,4]thiadiazole derivatives are the core structure of pharmacologically active molecules possessing antimicrobial, anticonvulsant, diuretic, anticancer, antitubercular, analgesic, and anti-inflammatory properties.[17c, 18] However, they have never been combined with a diagnostic tool, therefore appending this scaffold to an MRI agent would enable the generation of original companion diagnostics.

In this context, we have synthesized two new ligands containing an imidazo[2,1-*b*][1,3,4]thiadiazole heterocycle, linked to a DOTA monoamide macrocycle for Ln^{3+} complexation (Scheme 1). The two ligands differ by the position of the substitution on the imidazole moiety, either in position *C-5* or *C-6*. We have studied the properties of the heterocycles linked to the macrocycle, more precisely the protonation constants of the heterocycles by absorption, luminescence spectroscopy, as well as by pH-potentiometric titrations. We have investigated the photophysical properties of the corresponding Tb^{3+} complexes, as well as the relaxation properties of the Gd^{3+} analogues.

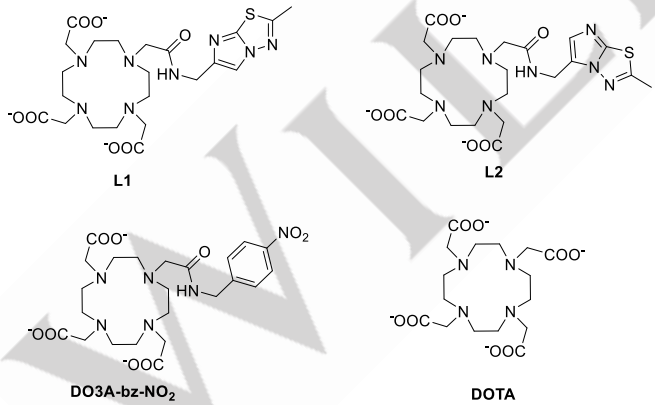

Scheme 1. Ligands discussed in this work.

Results and Discussion

Synthesis of the ligands

The synthetic pathways to obtain L1 and L2 are presented Scheme 2. First, we focused our attention on the amine derivatives **5** and **11**, which can be prepared by using short steps from commercially available 2-amino-5-methyl-1,3,4-thiadiazole **1**. The condensation of **1** and ethyl bromopyruvate led to ester **2** in moderate 24% yield. In the next step, treatment of **2** with DIBAL-H generated alcohol **3** in 51% of yield. Azidation of primary alcohol with DPPA followed by Staudinger reduction furnished amine **5**. To access to amine derivative **11**, a similar synthetic pathway was undertaken. The condensation of **1** with chloroacetyl chloride furnished **7** in 22% yield. Regioselective formylation in C-5 position using Vilsmeier-Haack conditions led to compound **8** in 54% of yield which was reduced in the presence of $NaBH_4$ to generate alcohol **9**. Facile conversion of alcohol **9** to primary amine **11** was realized in a two step sequence involving azidation and Staudinger reduction, once again, in satisfying yields. Amide bond formation of **5** and **11** with chloroacetyl chloride in presence of K_2CO_3 as base was performed to afford the expected chloro derivatives **6** and **12**. Finally, ligands **L1** and **L2** have been synthesized after the *N*-alkylation of DO3AtBu with chloro derivatives **6** and **12** following by a treatment of the crude with HCl 10N. **L1** and **L2** were isolated in 10% and 33% yields, respectively. The ^{1}H and ^{13}C NMR spectra of the various compound are presented Fig S1-11.

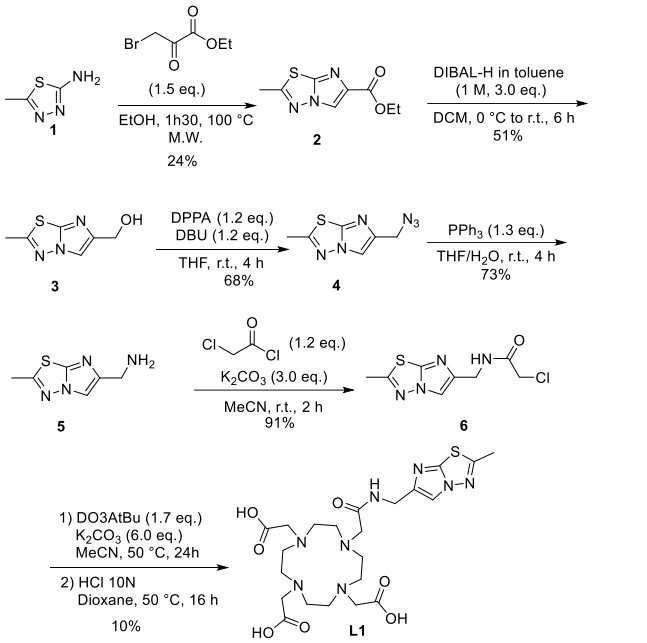

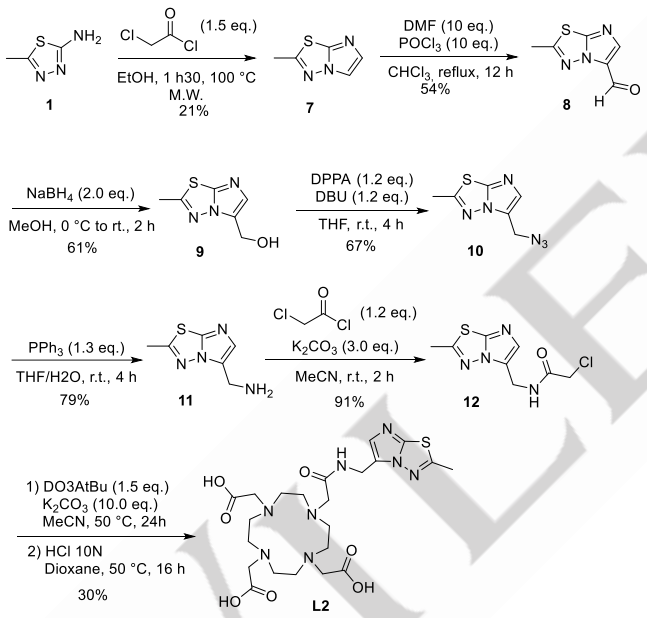

Scheme 2. Synthesis of Ligands L1 and L2.

Protonation constants of the ligands

The protonation constants of L1 and L2 were first determined by photophysical measurements. The absorption spectra of L1 and L2 at pH 7.4 in HEPES are presented Figure 1. Both ligands show broad bands up to 320 nm with slightly higher ε values for L2 compared to L1 in the 200-300 nm range. Emission and excitation spectra were also recorded at physiological pH and are presented in Figure S12 and S13.

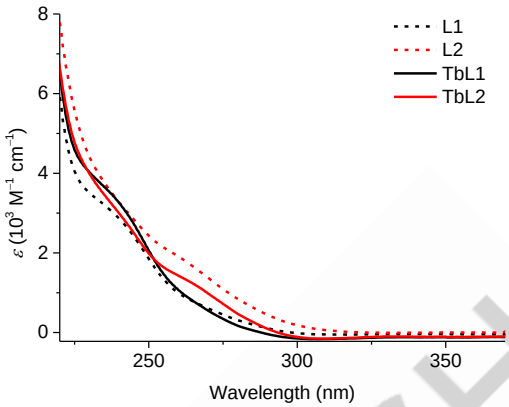

Figure 1. Absorption spectra of L1 and L2, and the corresponding Tb^{3+} complexes at 0.5 mM in HEPES pH 7.4, room temperature.

In order to determine the protonation constants of the heterocycle, we recorded the UV, fluorescence emission and excitation spectra of L1 and L2 in 0.1 M NaCl, at 25°C, in the pH range 3-11.5. The results are presented Figure 2 and S14-S17. Using HypSpec, the data was best-fitted to give two protonation constants that correspond to the protonation of the nitrogens of each heterocycle, and is presented in Table 1. It should be noted that in the case of L1, the changes in the excitation spectra over the pH range were not significant enough to obtain reliable values. For both ligands, the results obtained are consistent using UV, excitation and emission (when available) data. Both ligands have two protonation constants, a high one, above 8, and a lower one (around 4) which correspond to the protonation of the nitrogen atoms from the thiadiazole core, and the imidazole moiety. These protonation constants are not strongly affected by the different substitution on the heterocycle (L1 vs L2).

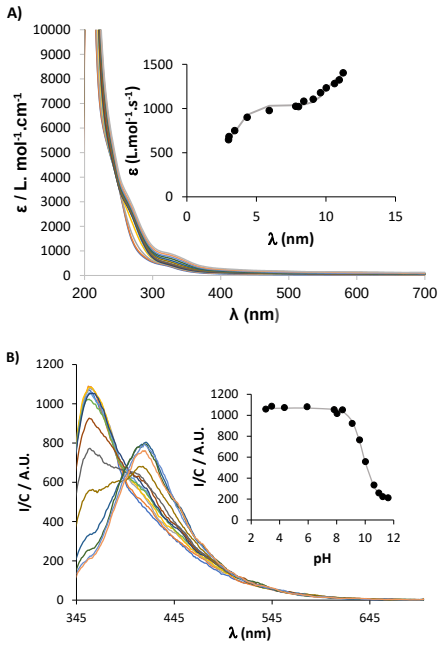

Figure 2. A) Absorption spectra of L2 (0.2 mM) in NaCl 0.1 M at 25°C ; inset : molar absoprtion coefficients at 292 nm as a function of pH. B) Emission spectra of L2 (0.2 mM) in NaCl 0.1 M (λ_{exc} = 315 nm) at 25°C ; inset : emission intensities at 360 nm as a function of pH. The lines represent the best fit and the corresponding values are given in Table 1.

Table 1. Protonation constants of L1 and L2 determined by absorption, and fluorescence in NaCl 0.1 M at 25°C.

	L1		L2		
	UV	**Emission**	**UV**	**Emission**	**Excitation**
Log K_{H1}	8.9 (3)	8.4 (2)	9.9 (1)	9.9 (1)	9.9 (1)
Log K_{H2}	4.5 (3)	4.3 (3)	3.9 (2)	4.0 (2)	4.5 (4)

Potentiometric measurements were also performed in NaCl 0.15 M for L2. This data was fitted to determine the protonation constants of the ligand, and compared to those of DOTA at different ionic strengths. The results are presented in Table 2 and Figure S18. L2 displays eight protonation constants. Three protonation constants are higher than 8.5, and two of them can be attributed to the protonation of the nitrogen atoms in the *trans* position of the macrocycle, while the third one can be attributed to the heterocycle. The value found is lower than that determined by photophysical measurements. However, it should be noted that the ionic strength in both experiments is not exactly the same (0.1 M for the photophysical measurements and 0.15 M for the potentiometric titrations). The protonation constants of the macrocycle are highly sensitive to ionic strength (see Table 1), which is consistent with the complexation of Na^+ in the macrocycle as previously demonstrated.[19] These values will in turn influence the protonation constant of the heterocycle, which could explain the lower value found by photophysical measurements. The fifth protonation constant fits well with the protonation of the second nitrogen of the heterocycle found by photophysical measurements. The other protonation constants correspond to the protonation of the carboxylates and/or the remaining nitrogens of the macrocycle.

Finally, the different substitutions on the heterocycle result in different photophysical features for the two ligands and as expected different protonation constant of the nitrogen from the imidazole ring.

Table 2. Protonation constants measured by potentiometric titrations at 298 K.

	L2	**DOTA[a]**	**DOTA[b]**
	0.15 M NaCl	0.1 M NaCl	1 M NaBr
Log K_{H1}	9.1 (1)	9,37	9.01
Log K_{H2}	8.98 (6)	9.14	9.08
Log K_{H3}	8.51 (1)	4.63	4.44
Log K_{H4}	4.77 (5)	3.91	3.74
Log K_{H5}	3.97 (3)		1.72
Log K_{H6}	3.76 (5)		
Log K_{H7}	2.33 (4)		
Log K_{H8}	2.1 (1)		

[a] From ref ; [b] From ref [20].

Photophysical properties

The absorption spectra of Tb^{3+} complexes were similar to that of the L1 and L2 ligands (Figure 1, S19), and present broad bands in the UV range up to 300 nm (Figure S2). Excitation spectra collected upon monitoring the Tb^{3+} emission at 545 nm are dominated by broad bands in the UV range (Figure 3, top) reflecting the ability of the imidazothiodiazole-based chromophores to sensitize luminescence of this Ln^{3+} through the 'antenna effect'.[21] In addition, in the excitation spectra, sharp features corresponding to Tb^{3+} f-f transitions are observed throughout the UV and visible ranges. Such results reflect that the direct excitation of Tb^{3+} is in competition with their antenna-sensitized excitation, as a strong indication of the limited efficiency of the imidazothiodiazole-based chromophores to transfer energy to the accepting levels of Tb^{3+}. Upon excitation into the ligand-centered bands at 270 nm TbL1 and TbL2 exhibit green emission with sharp features in the range of 480–700 nm due to the $^5D_4 \rightarrow {}^7F_J$ (J = 6–0) transitions of Tb^{3+} in addition to broader ligand-centered bands located at shorter wavelengths (Figure 3, bottom). Tb^{3+}-centered quantum yields were found to be very similar for TbL1 and TbL2, i.e. (0.021±0.002)% and (0.016±0.001)%. This relatively small value could be partially explained by the low efficiency of these chromophores to operate as Tb^{3+} sensitizers. In order to estimate the number of water molecules coordinated to Tb^{3+} using phenomenological equations,[22] luminescence decays for solutions of TbL1 and TbL2 in HEPES buffer (pH = 7.4) and D_2O (pD = 7.4) were acquired and analyzed. It was found that they are best fitted by bi-exponential functions (Table S1) as an indication of more than a single source of quenching. Average luminescence lifetime values are (1.5±0.1) ms and (1.9±0.1) ms for TbL2 in HEPES buffer and D_2O, respectively, and are the same, i.e. (1.3±0.1) ms, in both solutions for TbL1. Using these data, calculations reveal that no water molecules are coordinated to Tb^{3+} in TbL1 while the value of q = 0.4 was found for TbL2. This is surprising as such Ln-DOTA-monoamide complexes are expected to be monohydrated, which was confirmed by temperature dependent ^{17}O measurements (vide infra). This contradictory observation could be explained by the very low Tb^{3+} luminescence intensities that render the determination of the q values using phenomenological equations with luminescence lifetimes unreliable.

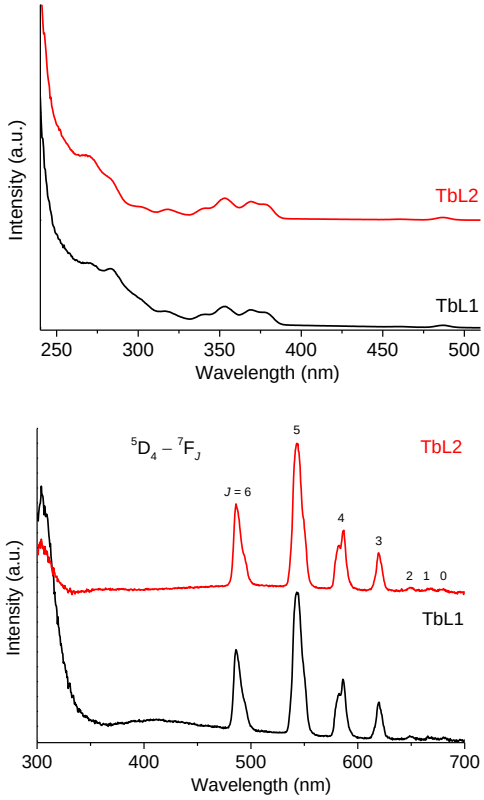

Figure 3. Photophysical results obtained for 0.5 mM solutions of Tb^{3+} complexes (HEPES buffer, pH 7.4, room temperature). (Top) Corrected and normalized to the intensity of the $^5L_9 \leftarrow {}^7F_6$ transition at 353.5 nm excitation spectra upon monitoring emission at 543 nm and (bottom) corrected and normalized to the intensity of the $^5D_4 \rightarrow {}^7F_5$ transition at 543 nm emission spectra upon excitation at 270 nm.

Relaxivity studies

To characterize the relaxivity of the corresponding Gd^{3+} complexes of L1 and L2, Paramagnetic Relaxation Enhancements (PRE) were measured at 60 MHz and 25°C as a function of concentration (Figure 4 and S20). The PRE are linear with the concentration, which shows the absence of aggregates in the concentration range studied. The slope of the line gives the relaxivity values of the complexes. Relaxivities of 4.58 $mM^{-1}.s^{-1}$ and 4.50 $mM^{-1}.s^{-1}$ were found for GdL1 and GdL2, respectively, meaning that the position of the substitution of the heterocycle does not have a strong influence on the relaxation properties of the complexes. These relaxivity values are higher than those of GdDOTA measured in the same conditions (r_1 = 3.70 $mM^{-1}.s^{-1}$ at 60 MHz, 25°C).

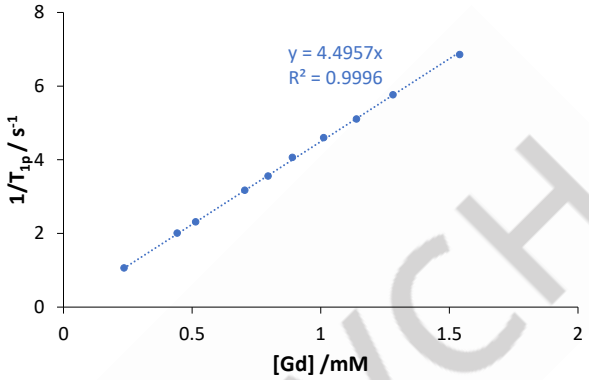

Figure 4. Paramagnetic Relaxation Enhancements measurements in the presence of GdL2 at 60 MHz and 25°C.

To characterise the parameters governing proton relaxivity of the complex, nuclear magnetic relaxation dispersion (NMRD) profiles were recorded in the field range 10 kHz-400 MHz, at three different temperatures. Since the relaxivity is determined by several physicochemical parameters, including water exchange rate, electron relaxation parameters and rotational correlation times, it is important to assess the maximum of these parameters independently. To this end, NMRD measurements are usually combined with ^{17}O NMR spectroscopy.

Variable temperature ^{17}O T_2 measurements give access to the water exchange rate, k_{ex}. The ^{17}O T_1 data is determined by dipole-dipole and quadrupolar relaxation mechanisms and provide information about the rotational correlation time, τ_R. The ^{17}O chemical shifts gives indication of the number of water molecules directly coordinated to Gd^{3+}, q. Longitudinal, transverse ^{17}O relaxation rates and chemical shifts were measured as a function of the temperature on aqueous solutions of GdL1 and GdL2, and on a diamagnetic reference ($HClO_4$, pH 3.3) at 9.4 T. The longitudinal relaxation rates measured for GdL1 and GdL2 were too close to those of the reference and were therefore excluded from the analysis. The reduced ^{17}O transverse relaxation rates and chemical shifts are presented in Figure 5.

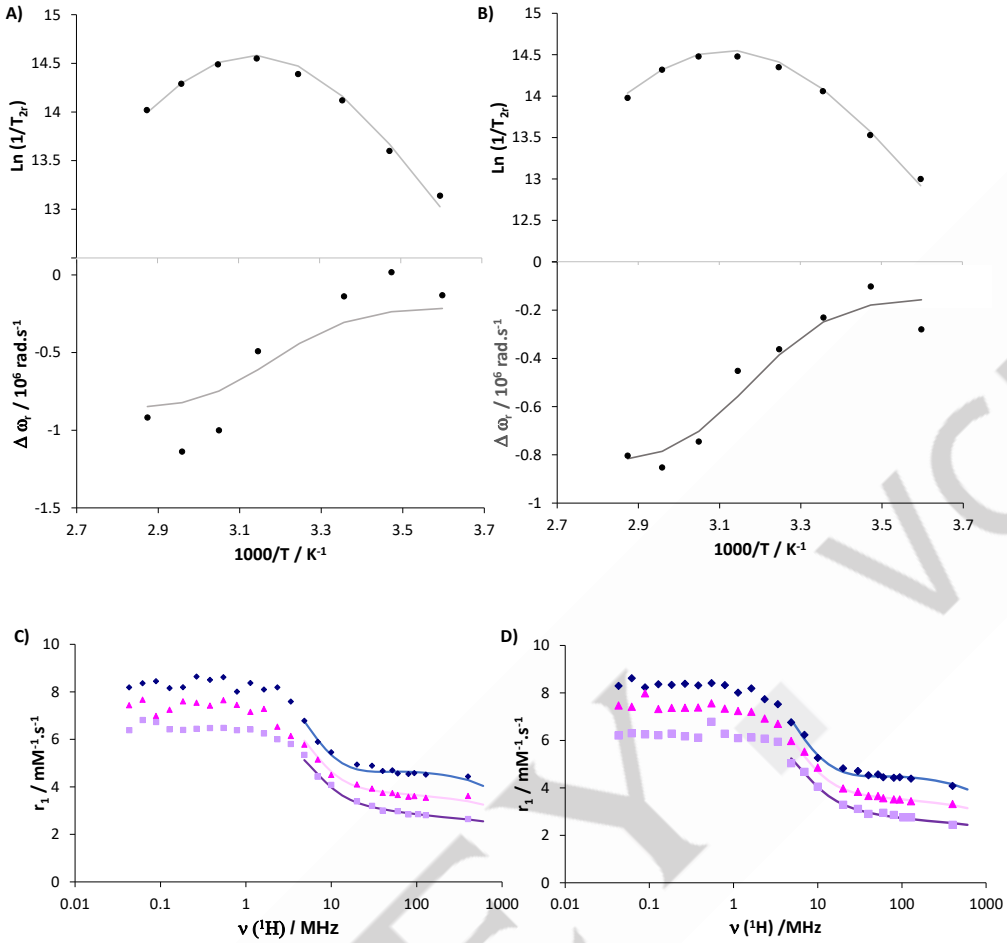

Figure 5. Temperature dependence of the reduced ^{17}O transverse relaxation rates (top), chemical shifts (middle) of GdL1 (A) and GdL2 (B) at 9.4 T. NMRD profiles of GdL1 (C) and GdL2 (D) at 25°c (blue ♦), 37°C (pink ▲), and 50°C (purple ■). The curves represent the simultaneous fit to the experimental data points.

The experimental values of the reduced ^{17}O chemical shifts measured both on GdL1 and GdL2, which are directly proportional to *q*, show that both complexes are monohydrated, as expected for such design. The reduced transverse relaxation rates ($1/T_{2r}$) can give access to the water exchange rate. For GdL1 and GdL2, the ^{17}O-reduced transverse relaxation rates first increase (up to *ca.* 320 K), then decrease with increasing temperature. It indicates that the complexes are in the slow kinetic region at low temperatures and in the fast exchange region at higher temperatures (Figure 5 top). In the slow kinetic region, $1/T_{2r}$ is directly determined by the exchange rate constant k_{ex}, whereas in the fast exchange region, it is determined by the transverse relaxation rate of the coordinated water oxygen, $1/T_{2m}$, which is in turn influenced by the water exchange rate, k_{ex}, the longitudinal electronic relaxation rate, $1/T_{1e}$, and the scalar coupling constant, A/ħ. In our case, the slow kinetic region is well-defined and enables a reliable determination of k_{ex}.

The transverse and longitudinal ^{17}O relaxation rates, and the NMRD profiles, were simultaneously analysed with the Solomon-Bloembergen and Morgan (SBM) theory to yield the microscopic parameters characterising water exchange and rotation (see ESI for equations). Indeed, if we are not interested in detailed information about the electron spin relaxation and if we restrict the analysis of the NMRD data to medium and high magnetic fields, the SBM approach gives reliable information on dynamic processes like water exchange and rotational correlation times for small complexes.[23] Therefore we decided to include only relaxivity values above 6 MHz in the fitting process.

In the analysis of the data, several parameters have been fixed to common values. Among these, r_{GdO} was fixed to 2.5 Å, based on available crystal structures and ENDOR results,[1] and the quadrupolar coupling constant, $\chi(1+\eta^2/3)^{1/2}$, was set to the value for pure water, 7.58 MHz.[24] The diffusion coefficients D_{GdH}^{298} = 26.10^{-9} $m^2.s^{-1}$ were fixed, and the corresponding activation energies E_{DGdH} were fitted. The Gd-water proton distance was fixed to r_{GdH} = 3.1Å, and the closest approach between the Gd^{3+} ion and the outer sphere protons was fixed to a_{GdH} = 3.6 Å. The values of the chemical shift measured are characteristic of a monohydrated complex. A hydration number of *q* = 1 was considered in all cases, and the following parameters have been adjusted: the water exchange rate, k_{ex}^{298}, the activation enthalpy for water exchange, $\Delta H^{\neq}$, the scalar coupling constant, *A*/ħ, the rotational correlation time, τ_R^{298}, and its activation energy, E_R, the empirical constant describing the outer sphere contribution to the ^{17}O chemical shift, C_{os}, and the parameters describing electron spin relaxation, the mean square of the zero field splitting, Δ^2, the correlation time for the modulation of the zero field splitting, τ_V^{298}, while its activation energy, E_V has been fixed to 1 kJ/mol. The parameters resulting from the best fit are presented in Table 3 and S2.

The fit yielded the values of k_{ex} of 2.2×10^6 s^{-1} for GdL1 and 2.0×10^6 s^{-1} for GdL2. This is lower than that of GdDOTA (k_{ex} = 4.1×10^6 s^{-1})[25] and in the same order of magnitude than another DOTA-monoamide complex (k_{ex} = 1.6×10^6 s^{-1}).[26] In the case of dissociative exchange for all DTPA- and DOTA-derivatives, it was generally observed that the replacement of one negatively charged carboxylate in the complex with a neutral amide decreases the exchange rate to about one third.[27] This rule applies here for GdL1 and GdL2. The relaxivity profiles as a function of temperature show a decrease of relaxivity with increasing temperature (Figure 5 bottom), which means that the relaxivity is limited by fast rotation. The fitted value of t_R are 98 ps and 92 ps for GdL1 and GdL2, respectively. They are higher than that of GdDOTA, which is consistent with the bigger size of those complexes.

Table 3. Parameters obtained from the simultaneous fitting of the transverse ^{17}O NMR relaxation rates and chemical shifts as a function of temperature at 9.4 T, and of the NMRD profiles at 298 K, 310 K, and 323 K, using the Solomon Bloembergen and Morgan theory presented in ESI.

	GdL1	GdL2	GdDOTA[a]	Gd(DO3A-bz-NO_2)[b]
k_{ex}^{298} ($10^6 s^{-1}$)	2.2 (2)	2.0 (1)	4.1	1.6
$\Delta H^{\neq}$ ($kJ.mol^{-1}$)	49 (3)	49 (2)	47.6	40.9
τ_R^{298} (ps)[a],[b]	98 (2)	92 (2)	77	210
E_R ($kJ.mol^{-1}$)	17 (2)	18 (2)	16.1	17.7
A/ħ ($10^6 rad.s^{-1}$)	-3.8 (2)	-3.6 (2)	-3.7	-3.8
Cos	0.23 (7)	0.16 (4)	0.21	0.06

[a] From ref [25]. [b] From ref [26]

Finally, the pH dependence of the relaxivity was checked for both complexes and the results are presented Figure 6.

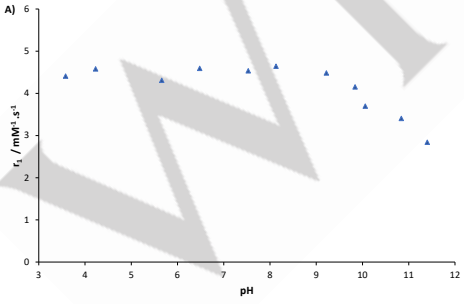

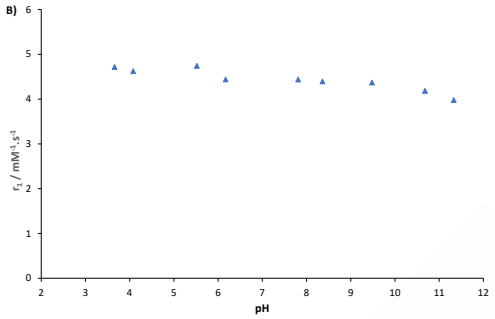

Figure 6. Relaxivity of GdL1 (A) and GdL2 (B) measured as a function of pH

The relaxivity is constant in the pH range 3 – 9 for both complexes, meaning that the protonation constants of the heterocycle do not affect the relaxivity values. Interestingly, the relaxivity remains constant for GdL2 up to pH 11, while a decrease is observed for GdL1. This could be explained by the formation of a hydroxo-complex, likely through the deprotonation of a water molecule. This hydroxo-complex would form at lower pH for GdL1 than for GdL2, which could be explained by different H-bonding networks in the two complexes.

Conclusion

In conclusion, we have developed efficient routes to the synthesis of DO3A-imidazo[2,1-*b*][1,3,4]thiadiazole complexes from readily accessible starting materials. The different substitution of the heterocycle does not influence strongly the protonation constant of this heterocycle. The ligands, as well as the corresponding Tb^{3+} complexes, display broad absorption bands in the UV-region. The imidazothiadiazole is able to sensitize Tb^{3+}-centered luminescence in both complexes with modest quantum yields. Such values reflect the limited efficiency of these chromophores to operate as sensitizers for Tb^{3+} combined with the non-radiative quenching of the luminescence of Tb^{3+} by the overtones of the water molecule coordinated to the metal ion. The corresponding monohydrated Gd^{3+} complexes display higher relaxivity than GdDOTA, mainly due to the larger size of the system. The water exchange rate of both complexes is consistent with that of other GdDOTA-monoamide complexes, proving that the presence of the bulky heterocycle does not influence this water exchange rate. Interestingly, no aggregation processes are observed in the concentration range studied by relaxivity. Finally, the substitution in the C5 or C6 position of the heterocycle does not influence neither the luminescence properties of the system, nor the relaxation properties, which are optimised compared to the gold standard, GdDOTA. These systems containing original heterocycle represent therefore an interesting platform for the development of theranostic systems.

Experimental section

General Information. ^{1}H NMR and ^{13}C NMR spectra were recorded on a Bruker DPX 400 MHz instrument using $CDCl_3$ and DMSO–d_6 or on a Bruker Advance III HD Spectrometer at 298 K using a 5 mm BBFO probe. ^{1}H and ^{13}C spectra were obtained respectively at 600 MHz and 150 MHz. The chemical shifts are reported in parts per million (*δ* scale), and all coupling constant (*J*) values are reported in hertz. The following abbreviations were used for the multiplicities: s (singlet), d (doublet), t (triplet), q (quartet), p (pentuplet), m (multiplet), sext (sextuplet), and dd (doublet of doublets). All compounds were characterized by ^{1}H NMR, and ^{13}C NMR which are consistent with those reported in the literature (Supplementary Materials). Melting points are uncorrected. IR absorption spectra were obtained on a PerkinElmer PARAGON 1000 PC, and the values are reported in inverse centimeters. HRMS spectra were acquired in positive mode with an ESI source on a Q–TOF mass by the "Fédération de Recherche" ICOA/CBM (FR2708) platform and NMR data were generated on the Salsa platform. Monitoring of the reactions was performed using silica gel TLC plates (silica Merck 60 F 254). Spots were visualized by UV light (254 nm and 356 nm). Column chromatography was performed using silica gel 60 (0.063–0.200 mm, Merck). Microwave irradiation was carried out in sealed vessels placed in a Biotage Initiator or Biotage Initiator+ system (400 W maximum power). The temperatures were measured externally by IR. Pressure was measured by a non–invasive sensor integrated into the cavity lid. All reagents were purchased from commercial suppliers and were used without further purification.

Synthesis and characterization.

Ethyl 2-methylimidazo[2,1-*b*][1,3,4]thiadiazole-6-carboxylate 2. The reaction was carried out as described in general procedure 1 using ethyl bromopyruvate (5.01 mL, 39.66 mmol, 1.5 eq.) and 5-methyl-1,3,4-thiadiazol-2-amine (3.045 g, 26.44 mmol, 1.0 eq.) in ethanol (30 mL). The crude mixture was purified by flash chromatography on silica gel (EP/EtOAc, 30/70) to afford compound **2** as a yellow solid (497 mg, 24%). *Spectral data corresponded to literature.*

(2-methylimidazo[2,1-*b*][1,3,4]thiadiazol-6-yl)methanol) 3. To a solution of Compound 2 (579 mg, 2.74 mmol, 1.0 eq) in DCM (56 mL) at 0 °C was added dropwise DIBAL-H in toluene (1N, 8.22 mL, 8.22 mmol, 3.0 eq). Reaction mixture was stirred for 6 h at room temperature before quenching with a saturated solution of Rochelle's salt. Resulting mixture was extracted three times with EtOAc and gathered organic fractions were concentrated and dried to afford compound **3** as a yellow solid (224 mg, 51%). Mp = 111-113 °C.^{1}H NMR (400 MHz, DMSO-*d6*) δ (ppm): 7.87 (s, 1H), 5.06 (t, *J* = 5.7 Hz, 1H), 4.42 (d, *J* = 5.2 Hz, 2H), 2.69 (s, 3H).; ^{13}C NMR (101 MHz, DMSO-d_6) δ (ppm): 159.75, 147.43, 143.70, 110.91, 58.08, 17.38.; HRMS (EI-MS) m/z calcd for $C_6H_8N_3OS$: 170.0386 $[M+H]^+$, found: 170.0383.

(6-(azidomethyl)-2-methylimidazo[2,1-*b*][1,3,4]thiadiazole) 4. The reaction was carried out as described in general procedure 2 using Compound 3 (407 mg, 2.41 mmol, 1.0 eq), DBU (0.4 mL, 2.88 mmol, 1.2 eq) and DPPA (0.6 mL, 2.88 mmol, 1.2 eq) in THF (45 mL). The crude mixture was purified by flash chromatography on silica gel (EP/EtOAc, 70/30) to afford compound **4** as an off-white solid (316 mg, 68%). Mp = 62-64 °C.^{1}H NMR (400 MHz, DMSO-*d6*) δ (ppm): 8.14 (s, 1H), 4.36 (s, 2H), 2.71 (s, 3H).; ^{13}C NMR (101 MHz, DMSO-d_6) δ (ppm): 160.97, 144.89, 140.34, 112.82, 47.91, 17.41.; HRMS (EI-MS) m/z calcd for $C_6H_7N_6S$: 195.0449 $[M+H]^+$, found: 195.0447.

(2-methylimidazo[2,1-*b*][1,3,4]thiadiazol-6-yl)methanamine) 5.

The reaction was carried out as described in general procedure 3 using Compound 4 (116 mg, 0.60 mmol, 1.0 eq) and PPh_3 (204 mg 0.77 mmol 1.3 eq) in a mixture of THF/H_2O (10/1 mL). The crude mixture was purified by flash chromatography on silica gel (DCM/MeOH, 90/10) to afford compound **5** as a light-yellow solid (74 mg, 73%). Mp = 62-64 °C. ^{1}H NMR (400 MHz, DMSO-*d6*) δ (ppm): 7.83 (s, 1H), 3.66 (s, 2H), 2.69 (s, 3H).; ^{13}C NMR (101 MHz, DMSO-d_6) δ (ppm): 159.43, 149.23, 143.56, 109.94, 40.42, 17.35.; HRMS (EI-MS) m/z calcd for $C_6H_9N_4S$: 195.0449 $[M+H]^+$, found: 195.0447.

(2-chloro-N-((2-methylimidazo[2,1-*b*][1,3,4]thiadiazol-6-yl)methyl)acetamide) 6. The reaction was carried out as described in general procedure 4 using Compound 5 (50 mg, 0.3 mmol, 1.0 eq), chloroacetyl chloride (0.3 ml, 0.36 mmol, 1.2 eq) and K_2CO_3 (125 mg, 0.9 mmol, 3.0 eq) in MeCN (5 mL). The crude mixture was purified by flash chromatography on silica gel (DCM/AcOEt, 40/60) to afford compound **6** as an off-white solid (67 mg, 91%). Mp = 110-112 °C. ^{1}H NMR (400 MHz, DMSO-*d6*) δ (ppm): 8.60 (t, *J* = 5.4 Hz, 1H), 7.90 (s, 1H), 4.27 (d, *J* = 5.5 Hz, 2H), 4.09 (s, 2H), 2.70 (s, 3H).; ^{13}C NMR (101 MHz, DMSO-d_6) δ (ppm): 165.67, 160.20, 143.94, 143.09, 111.36, 42.56, 37.66, 17.37.; HRMS (EI-MS) m/z calcd for $C_6H_{10}ClN_4OS$: 245.0269 $[M+H]^+$, found: 245.0258.

(2-methylimidazo[2,1-*b*][1,3,4]thiadiazole) 7. The reaction was carried out as described in general procedure 1 using chloroacetaldehyde (50% wt. % in water, 1.62 mL, 13.2 mmol, 1.5 eq) and 5-methyl-1,3,4-thiadiazol-2-amine (1.017 g, 8.8 mmol, 1.0 eq) in ethanol (15 mL). The crude mixture was purified by flash chromatography on silica gel (EP/EtOAc, 30/70) to afford compound 7 as a white solid (260 mg, 21%). *Spectral data corresponded to literature.*

(2-methylimidazo[2,1-*b*][1,3,4]thiadiazole-5-carbaldehyde) 8. To a mixture of DMF (4.5 mL) and Chloroform (2 mL) at 0 °C under argon was added $POCl_3$ (10 eq, 2.4 mL, 25 mmol) dropwise. The reaction mixture was stirred at 0 °C for 10 min under argon before Compound 7 (1 eq, 351 mg, 2.5 mmol) in Chloroform (11 mL) was added dropwise. Reaction mixture was stirred under argon for 30 min at rt and then 16 h under reflux. After cooling down to rt, the reaction mixture was added dropwise to an ice-water solution. The latter was extracted 4x with DCM, washed with Brine, dried over $MgSO_4$ and evaporated to yield expected compound **8** (228 mg, 54%) as a pale brown solid. Mp = 166-168 °C. ^{1}H NMR (400 MHz, $CDCl_3$) δ (ppm): 9.89 (s, 1H), 8.00 (s, 1H), 2.83 (s, 3H).; ^{13}C

NMR (101 MHz, $CDCl_3$) δ (ppm): 176.28, 163.00, 152.46, 144.23, 128.28, 18.21.; HRMS (EI-MS) m/z calcd for $C_6H_6N_3OS$: 168.0229 $[M+H]^+$, found: 168.0226.

(2-methylimidazo[2,1-*b*][1,3,4]thiadiazol-5-yl)methanol) 9. To a solution of Compound 8 (1 eq, 377 mg, 2.2 mmol) in MeOH (15 mL) was added $NaBH_4$ (2 eq, 170 mg, 4.5 mmol) portion wise at 0 °C and the reaction mixture was stirred at rt under argon for 3 h. Volatiles were removed under vacuum, suspended in water, extracted three times with AcOEt, dried over $MgSO_4$ and evaporated to yield expected product **9** as a pale brown solid (235 mg, 61%). Mp = 170-172 °C. ^{1}H NMR (400 MHz, DMSO-*d*$_6$) δ (ppm): 7.14 (s, 1H), 5.22 (t, *J* = 5.4 Hz, 1H), 4.64 (d, *J* = 5.2 Hz, 2H), 2.72 (s, 3H).; ^{13}C NMR (101 MHz, DMSO-*d*$_6$) δ (ppm): 160.69, 143.31, 130.93, 127.55, 52.37, 17.46.; HRMS (EI-MS) m/z calcd for $C_6H_8N_3OS$: 170.0384 $[M+H]^+$, found: 170.0383.

(5-(azidomethyl)-2-methylimidazo[2,1-*b*][1,3,4]thiadiazole) 10. The reaction was carried out as described in general procedure 2 using compound 9 (523 mg, 3.1 mmol, 1.0 eq), DBU (0.6 mL, 3.7 mmol, 1.2 eq) and DPPA (0.8 mL, 3.7 mmol, 1.2 eq) in THF (47 mL). The crude mixture was purified by flash chromatography on silica gel (EP/EtOAc, 70/30) to afford compound **10** as an off-white solid (316 mg, 67%). Mp = 60-60 °C. ^{1}H NMR (400 MHz, DMSO-*d*$_6$) δ (ppm): 7.33 (s, 1H), 4.72 (s, 2H), 2.74 (s, 3H).; ^{13}C NMR (101 MHz, DMSO-*d*$_6$) δ (ppm): 161.93, 132.94, 132.80, 120.41, 43.15, 17.39.; HRMS (EI-MS) m/z calcd for $C_6H_7N_6S$: 195.0449 $[M+H]^+$, found: 195.0447.

(2-methylimidazo[2,1-*b*][1,3,4]thiadiazol-5-yl)methanamine) 11. The reaction was carried out as described in general procedure 3 using Compound 10 (368 mg, 1.9 mmol, 1.0 eq) and PPh_3 (645 mg 2.5 mmol 1.3 eq) in a mixture of THF/H_2O (30/3 mL). The crude mixture was purified by flash chromatography on silica gel (DCM/MeOH, 90/10) to afford compound **11** as a light-yellow solid (250 mg, 79%). Mp = 59-61 °C. ^{1}H NMR (400 MHz, DMSO-*d*$_6$) δ (ppm): 7.05 (s, 1H), 3.90 (s, 2H), 2.72 (s, 3H).; ^{13}C NMR (101 MHz, DMSO-*d*$_6$) δ (ppm): 160.42, 143.16, 129.26, 129.21, 35.45, 17.50.; HRMS (EI-MS) m/z calcd for $C_6H_9N_4S$: 169.0546 $[M+H]^+$, found: 169.0542.

(2-chloro-N-((2-methylimidazo[2,1-*b*][1,3,4]thiadiazol-5-yl)methyl)acetamide) 12. The reaction was carried out as described in general procedure 4 using Compound 11 (50 mg, 0.3 mmol, 1.0 eq), chloroacetyl chloride (0.3 ml, 0.36 mmol, 1.2 eq) and K_2CO_3 (125 mg, 0.9 mmol, 3.0 eq) in MeCN (5 mL). The crude mixture was purified by flash chromatography on silica gel (DCM/AcOEt, 40/60) to afford compound **12** as an off-white solid (70 mg, 91%). Mp = 174-175 °C. ^{1}H NMR (400 MHz, $CDCl_3$) δ (ppm): 7.21 (s, 1H), 7.05 (bs, 1H), 4.75 (d, *J* = 5.6 Hz, 2H), 4.08 (s, 2H), 2.72 (s, 3H).; ^{13}C NMR (101 MHz, $CDCl_3$) δ (ppm): 165.81, 160.77, 145.49, 131.93, 122.93, 42.69, 33.55, 18.05, 0.13.; HRMS (EI-MS) m/z calcd for $C_8H_{10}ClN_4OS$: 245.0263 $[M+H]^+$, found: 245.0258.

2,2',2''-(10-(2-(((2-methylimidazo[2,1-*b*][1,3,4]thiadiazol-6-yl)methyl)amino)-2-oxoethyl)-1,4,7,10-tetraazacyclododecane-1,4,7-triyl)triacetic acid) L1. Compound **6** (170 mg, 0.69 mmol, 1 eq) and K_2CO_3 (600 mg, 4.3 mmol, 6 eq) are added to a 15 mL solution of DO3A-tBu_3 (600 mg, 1.17 mmol, 1.7 eq) in anhydrous acetonitrile. The mixture was heated at 50 °C and stirred during 24 h. The resulting heterogeneous mixture was filtered, washed with 2x 5 mL of dichloromethane and the volatiles were evaporated under vacuum. The resulting yellow oil was dissolved in 5 mL of dioxane and 5 mL of (HCl 10N). The mixture was stirred during 16 h at 50 °C before volatiles were removed under vacuum and suspended in MilliQ water. The pH was increased to 4-5 with NaOH (2N) and resulting crude product was purified by flash chromatography on reversed phase with a gradient MilliQ water/MeOH (100:0 / 50:50 / 0:100) leading to **L1** as a white solid (38 mg, 10%). ^{1}H NMR (600 MHz, D_2O) δ (ppm): 7.77 (s, 1H), 4.39 (s, 2H), 3.26 (s, 2H), 3.09 – 2.88 (m, 6H), 2.77 – 2.27 (m, 19H).; ^{13}C NMR (151 MHz, D_2O) δ (ppm): 180.02, 173.69, 162.64, 145.81, 142.17, 111.68, 58.74, 57.64, 50.73, 37.19, 16.79.; HRMS (EI-MS) m/z calcd for $C_{22}H_{35}N_8O_7S$: 555.2344 $[M+H]^+$, found: 555.2347.

(2,2',2''-(10-(2-(((2-methylimidazo[2,1-b][1,3,4]thiadiazol-5-yl)methyl)amino)-2-oxoethyl)-1,4,7,10-tetraazacyclododecane-1,4,7-triyl)triacetic acid) L2. Compound **12** (134 mg, 0,55 mmol, 1 eq) and K_2CO_3 (735 mg, 5.3 mmol, 10 eq) are added to a 15 mL solution of DO3A-tBu_3 (423 mg, 0.82 mmol, 1.5 eq) in anhydrous acetonitrile. The mixture was heated at 50 °C and stirred during 24 h. The resulting heterogeneous mixture was filtered, washed with 2x 5 mL of dichloromethane and the volatiles were evaporated under vacuum. The resulting yellow oil was dissolved in 5 mL of dioxane and 5 mL of (HCl 10N). The mixture was stirred during 16 h at 50 °C before volatiles were removed under vacuum and suspended in MilliQ water. The pH was increased to 4-5 with NaOH (2N) and resulting crude product was purified by flash chromatography on reversed phase with a gradient MilliQ water/MeOH (100:0 / 50:50 / 0:100) leading to L2 as a white solid (91 mg, 30%). ^{1}H NMR (600 MHz, D_2O) δ (ppm): 7.38 (s, 1H), 4.63 (s, 2H), 3.91 – 3.79 (m, 4H), 3.64 – 2.99 (m, 12H), 3.21 – 3.03 (m, 8H), 2.78 (s, 3H).; ^{13}C NMR (151 MHz, D_2O) δ (ppm): 169.85, 124.19, 95.59, 56.47, 55.17, 54.13, 51.62, 50.80, 48.27, 48.14, 32.69, 16.87.; HRMS (EI-MS) m/z calcd for $C_{22}H_{35}N_8O_7S$: 555.2344 $[M+H]^+$, found: 555.2351.

Liquid sample preparation. The ligand concentrations were determined by adding an excess of zinc solution to a ligand solution and titrating the metal excess with standardized Na_2H_2EDTA in urotropine buffer (pH 5.6–5.8) in the presence of Xylenol Orange or Eriochrome Black T, or Murexide as indicators. The concentration of the metal solutions were determined similarly by complexometric titrations. The complexes were prepared by mixing 1 eq. of L, with 1 eq. of Ln^{3+}, and the pH was adjusted to 7.4 either with a buffered solution or by adding KOH or HCl to the solution. The absence of free Ln^{3+} was checked by the Xylenol orange test. The concentrations of Ln^{3+}-containing solutions were also checked both by ICP-MS and BMS measurements when possible.

Potentiometric Studies. Carbonate-free 0.1 M NaOH and 0.1 M HCl were prepared from Fisher Chemicals concentrates. Potentiometric titrations were performed in 0.15 mol. L^{-1} aqueous NaCl under nitrogen atmosphere and the temperature was controlled to 25±0.1 °C with a circulating water bath. The p[H] (p[H] = -log[H+], concentration in molarity) was measured in each titration with a combined pH glass electrode (Metrohm) filled with 3M KCl and the titrant addition was automated by use of a 702 SM titrino system (Metrohm). The electrode was calibrated in hydrogen ion concentration by titration of HCl with NaOH in 0.15 M electrolyte solution.[28] A plot of meter reading versus p[H] allows the determination of the electrode standard potential (E°) and the slope factor (f). Continuous potentiometric titrations with HCl and NaOH 0.1 M were conducted on aqueous solutions containing 5 mL of L 3.47 mM in NaCl 0.15 M, with 2 minutes waiting between successive points. The titrations of the metal complexes were performed with the same ligand solutions containing 1 or 2 equivalents of metal cation, with 2 minutes waiting time between 2 points. Experimental data was refined using the computer program Hyperquad 2008.[29] All equilibrium constants are concentration quotients rather than activities and are defined as:

$$K_{mhl} = \frac{[M_m L_l H_h]}{[M]^m [L]^l [H]^h}$$

The ionic product of water at 25 °C and 0.15 molL-1 ionic strength is pKw = 13.77.[30] Fixed values were used for pKw, ligand acidity constants and total concentrations of metal, ligand and acid. All values and errors (one standard deviation) reported are at least the average of three independent experiments.

Photophysical measurements. For the determination of the protonation constants, samples of [L1] = 0.47 mM, and [L2] =0.2 mM, were titrated with KOH, NaOH or HCl in NaCl 0.1 M. , UV-visible absorption spectra were recorded at 298 K on a Perkin Elmer UV/Vis/Nir Spectrometer Lambda 19 in the range λ = 200-500 nm with data steps of 1 nm, with a 1 cm path length. Luminescence measurements were performed at 298 K on an Agilent Cary Eclipse Fluorescence spectrophotometer with the following settings: excitation at 270 nm and emission scanning between 30 and 600 nm with an emission filter 295-1100nm, slit widths 5 nm for excitation and emission wavelengths. The data was treated with HypSpec.[29, 31] For photophysical measurements with Tb^{3+} complexes, 0.5 mM solutions in HEPES buffer (pH=7.4, 20mM) or D_2O (pD = 7.4) were prepared. For collecting photophysical data, samples were placed into 2.4 mm i.d. quartz capillaries or quartz Suprasil cells (Hellma® 115F-QS, bandpass 0.2 or 1 cm). Absorption spectra were measured on a Jasco V-670 UV/Visible/NIR spectrophotometer. Emission and excitation spectra were measured on a Horiba-Jobin-Yvon Fluorolog 3 spectrofluorimeter. All spectra were corrected for the instrumental functions. Luminescence lifetimes were determined under excitation at 266 nm provided by a YG 980 Quantel Nd:YAG laser while the Tb^{3+} signal was selected using an iHR320 monochromator (Horiba Scientific) and detected using a R928 photomultiplier tube (185-900 nm). The output signal from the detector was then fed to a Tektronix TDS 754C 500MHz bandpass digital oscilloscope and then transferred to a PC for treatment with Origin 9®. Luminescence lifetimes are averages of at least three independent measurements. Tb^{3+}-centered quantum yields were determined with a Fluorolog 3 spectrofluorimeter using an integration sphere (Model G8, GMP SA, Renens, Switzerland) and 0.1 mM solution of TbL_1 complex from Ref. [32] as a standard (Q_{Tb}^{L} = 37±1% in HEPES buffer, pH 7.4). Estimated experimental error for quantum yields determination is 10 %.Luminescence.

Relaxometric measurements. Proton NMRD profiles were recorded on a Stelar SMARTracer Fast Field Cycling relaxometer (0.01-10 MHz) and a Bruker WP80 NMR electromagnet adapted to variable field measurements (20-80 MHz) and controlled by a SMARTracer PC-NMR console. The temperature was monitored by a VTC91 temperature control unit and maintained by a gas flow. The temperature was determined by previous calibration with a Pt resistance temperature probe. The longitudinal relaxation rates ($1/T_1$) were determined in water.

Temperature dependent ^{17}O NMR measurements. The transverse and longitudinal ^{17}O NMR relaxation rates ($1/T_2$, $1/T_1$) and the chemical shifts were measured in aqueous solutions of **GdL** in the temperature range 278-348 K, on a Bruker Avance 400 (9.4 T, 54.5 MHz) spectrometer. The temperature was calculated according to previous calibration with ethylene glycol and methanol.[33] An acidified water solution ($HClO_4$, pH 3.3) was used as external reference. Transverse relaxation times (T_2) were obtained by the Carr-Purcell-Meiboom-Gill spin-echo technique.[34] The technique of the ^{17}O NMR measurements on Gd^{3+} complexes has been described elsewhere.[35] The samples were sealed in glass spheres fitted into 10 mm NMR tubes to avoid susceptibility corrections of the chemical shifts.[36] To improve the sensitivity ^{17}O-enriched water (10 % $H_2{}^{17}O$, CortectNet) was added to reach around 1 % enrichment. The concentrations of solutions were as follows: [**GdL1**] = 5.03 mM, and [**GdL2**] = 5.20 mM. The least-square fit of the ^{17}O NMR were performed using Visualiseur/Optimiseur[37] running on a MATLAB 8.3.0 (R2014a) platform.

Supporting Information

The authors have cited additional references within the Supporting Information.[38]

Acknowledgements

The authors would like to thank the Région Centre Val de Loire (RTR Motivhealth), the SFR neuroimagerie (SFR FED 4224), the fédération de recherche " Physique et chimie du vivant" FR CNRS 2708, the Labex programs SYNORG (ANR-11-LABX-0029) and IRON (ANR-11-LABX-0018-01), the Ligue contre le Cancer du Grand Ouest (comités des Deux Sèvres, du Finistère, de l'Ile et Villaine, du Loir et Cher, de Loire Atlantique, du Loiret, de la Vienne, du Morbihan, de l'Eure et Loire) and the Réseau 'Molécules Marines, Métabolisme & Cancer' du Cancéropôle Grand Ouest for their financial support. We also thank the SALSA and MO2VING platforms for spectroscopic measurements

spectrometric and chromatographic analyses (NMR, HPTLC, HPLC, MS, HRMS). S.P. acknowledges support from Institut National de la Santé et de la Recherche Médicale (INSERM).

Keywords: Probes • Magnetic resonance imaging • Luminescence • Sensitization • [5,5]-Fused Ring Systems •imidazothiadiazole

[1] P. Caravan, J. J. Ellison, T. J. McMurry, R. B. Lauffer, *Chem. Rev.* **1999**, *99*, 2293-2352.

[2] A. E. Merbach, L. Helm, E. Toth, *The Chemistry of Contrast Agents in Medical Magnetic Resonance Imaging*, Second Edition ed., John Wiley & Sons, Chichester, **2013**.

[3] Q. N. Do, R. E. Lenkinski, G. Tircso, Z. Kovacs, *Molecules* **2022**, *27*.

[4] C. S. Bonnet, E. Toth, *Comptes Rendus Chimie* **2010**, *13*, 700-714.

[5] a) J. Wahsner, E. M. Gale, A. Rodríguez-Rodríguez, P. Caravan, *Chem. Rev.* **2019**, *119*, 957-1057; b) S. Lacerda, K. Djanashvili, C. S. Bonnet, in *Supramolecular Chemistry in Biomedical Imaging* (Eds.: S. Faulkner, T. Gunnlaugsson, G. O Maille), The Royal Society of Chemistry, **2022**, p. 0.

[6] A. G. Robertson, L. M. Rendina, *Chem. Soc. Rev.* **2021**, *50*, 4231-4244.

[7] Shreyas P. Vaidya, S. Gadre, Ravi T. Kamisetti, M. Patra, *Biosci. Rep.* **2022**, *42*.

[8] a) J. Schmitt, S. Jenni, A. Sour, V. Heitz, F. Bolze, A. Pallier, C. S. Bonnet, E. Toth, B. Ventura, *Bioconjug. Chem.* **2018**, *29*, 3726-3738; b) S. Jenni, F. Bolze, C. S. Bonnet, A. Pallier, A. Sour, E. Toth, B. Ventura, V. Heitz, *Inorg. Chem.* **2020**, *59*, 14389-14398; c) L. Abad Galán, N. Hamon, C. Nguyen, E. Molnár, J. Kiss, J. Mendy, K. Hadj-Kaddour, M. Onofre, G. Trencsényi, C. Monnereau, M. Beyler, G. Tircsó, M. Gary-Bobo, O. Maury, R. Tripier, *Inorganic Chemistry Frontiers* **2021**, *8*, 2213-2224.

[9] S. L. Ho, H. Yue, T. Tegafaw, M. Y. Ahmad, S. Liu, S.-W. Nam, Y. Chang, G. H. Lee, *ACS Omega* **2022**, *7*, 2533-2553.

[10] S. Geninatti-Crich, D. Alberti, I. Szabo, A. Deagostino, A. Toppino, A. Barge, F. Ballarini, S. Bortolussi, P. Bruschi, N. Protti, S. Stella, S. Altieri, P. Venturello, S. Aime, *Chem. Eur. J.* **2011**, *17*, 8479-8486.

[11] T. L. Kalber, N. Kamaly, P.-W. So, J. A. Pugh, J. Bunch, C. W. McLeod, M. R. Jorgensen, A. D. Miller, J. D. Bell, *Molecular Imaging and Biology* **2011**, *13*, 653-662.

[12] J. Kaur, Y. Tsvetkova, K. Arroub, S. Sahnoun, F. Kiessling, S. Mathur, *Chemical Biology & Drug Design* **2017**, *89*, 269-276.

[13] K.-H. Jung, S.-H. Kang, M.-K. Kang, S. Kim, H.-K. Kim, Y.-H. Kim, G. Ho Lee, G.-B. Shim, J.-C. Jung, Y. Chang, T.-J. Kim, *Eur. J. Inorg. Chem.* **2015**, *2015*, 599-604.

[14] Z. Yang, H. Lin, J. Huang, A. Li, C. Sun, J. Richmond, J. Gao, *Chem. Commun.* **2019**, *55*, 4546-4549.

[15] B. Sung, H.-K. Kim, A.-R. Baek, B.-W. Yang, Y.-H. Kim, G. Choi, H.-J. Park, M. Kim, J. Lee, Y. Chang, *International Journal of Molecular Sciences* **2023**, *24*, 6870.

[16] F. Buron, M.-A. Hiebel, J.-Y. Mérour, K. Plé, S. Routier, in *Adv. Heterocycl. Chem., Vol. 125* (Eds.: E. F. V. Scriven, C. A. Ramsden), Academic Press, **2018**, pp. 301-356.

[17] a) J. Marco-Contelles, E. Pérez-Mayoral, P. Ballesteros, in *Comprehensive Heterocyclic Chemistry III* (Eds.: A. R. Katritzky, C. A. Ramsden, E. F. V. Scriven, R. J. K. Taylor), Elsevier, Oxford, **2008**, pp. 199-305; b) H. A. Mohamed, B. F. Abdel-Wahab, *Journal of Sulfur Chemistry* **2012**, *33*, 589-604; c) B. A. Bhongade, S. Talath, R. A. Gadad, A. K. Gadad, *Journal of Saudi Chemical Society* **2016**, *20*, S463-S475; d) S. Saba, in *Comprehensive Heterocyclic Chemistry II* (Eds.: A. R. Katritzky, C. W. Rees, E. F. V. Scriven), Pergamon, Oxford, **1996**, pp. 191-198.

[18] a) A. Cristina, D. Leonte, L. Vlase, L. C. Bencze, S. Imre, G. Marc, B. Apan, C. Mogoșan, V. Zaharia, in *Molecules, Vol. 23*, **2018**; b) N. Terzioglu, A. Gürsoy, *Eur. J. Med. Chem.* **2003**, *38*, 781-786; c) R. Romagnoli, P. G. Baraldi, F. Prencipe, J. Balzarini, S. Liekens, F. Estévez, *Eur. J. Med. Chem.* **2015**, *101*, 205-217; d) W. S. Alwan, R. Karpoormath, M. B. Palkar, H. M. Patel, R. A. Rane, M. S. Shaikh, A. Kajee, K. P. Mlisana, *Eur. J. Med. Chem.* **2015**, *95*, 514-525; e) H. M. Patel, B. Sing, V. Bhardwaj, M. Palkar, M. S. Shaikh, R. Rane, W. S. Alwan, A. K. Gadad, M. N. Noolvi, R. Karpoormath, *Eur. J. Med. Chem.* **2015**, *93*, 599-613; f) S. Cascioferro, G. Li Petri, B. Parrino, B. El Hassouni, D. Carbone, V. Arizza, U. Perricone, A. Padova, N. Funel, G. J. Peters, G. Cirrincione, E. Giovannetti, P. Diana, *Molecules* **2020**, *25*, 329.

[19] É. Tóth, R. Király, J. Platzek, B. Radüchel, E. Brücher, *Inorg. Chim. Acta* **1996**, *249*, 191-199.

[20] É. Csajbók, Z. Baranyai, I. Bányai, E. Brücher, R. Király, A. Müller-Fahrnow, J. Platzek, B. Radüchel, M. Schäfer, *Inorg. Chem.* **2003**, *42*, 2342-2349.

[21] J.-C. G. Bünzli, *Coord. Chem. Rev.* **2015**, *293-294*, 19-47.

[22] A. Beeby, I. M. Clarkson, R. S. Dickins, S. Faulkner, D. Parker, L. Royle, A. S. de Sousa, J. A. G. Williams, M. Woods, *J. Chem. Soc., Perkin Trans.* **1999**, 493-503.

[23] aP. H. Fries, E. Belorizky, *J. Chem. Phys.* **2005**, *123*, 124510; bP. Mieville, H. Jaccard, F. Reviriego, R. Tripier, L. Helm, *Dalton Trans.* **2011**, *40*, 4260.

[24] B. Halle, H. Wennerstrom, *The Journal of Chemical Physics* **1981**, *75*, 1928-1943.

[25] D. H. Powell, O. M. NiDhubhghaill, D. Pubanz, L. Helm, Y. S. Lebedev, W. Schlaepfer, A. E. Merbach, *J. Am. Chem. Soc.* **1996**, *118*, 9333-9346.

[26] É. Tóth, D. Pubanz, S. Vauthey, L. Helm, A. E. Merbach, *Chem. Eur. J.* **1996**, *2*, 1607-1615.

[27] E. Toth, L. Helm, A. Merbach, in *The Chemistry of Contrast Agents in Medical Magnetic resonance Imaging*, Second Edition ed. (Eds.: A. Merbach, L. Helm, E. Toth), John Wiley & Sons, Chichester, **2013**, pp. 25-81.

[28] A. E. Martell, R. J. Motekaitis, *Determination and use of stability constants*, VCH, **1992**.

[29] P. Gans, A. Sabatini, A. Vacca, *Talanta* **1996**, *43*, 1739-1753.

[30] R. M. Smith, R. J. Motekaitis, A. E. Martell, National Institute of standards and technology ed., NIST Standard Reference Database, **1997**.

[31] P. Gans, A. Sabatini, A. Vacca, *Ann. Chim. (Rome)* **1999**, *89*, 45-49.

[32] J. He, C. S. Bonnet, S. V. Eliseeva, S. Lacerda, T. Chauvin, P. Retailleau, F. Szeremeta, B. Badet, S. Petoud, E. Toth, P. Durand, *J. Am. Chem. Soc.* **2016**, *138*, 2913-2916.

[33] D. S. Raiford, C. L. Fisk, E. D. Becker, *Anal. Chem.* **1979**, *51*, 2050-2051.

[34] S. Meiboom, D. Gill, *Review of Scientific Instruments* **1958**, *29*, 688-691.

[35] K. Micskei, L. Helm, E. Brucher, A. E. Merbach, *Inorg. Chem.* **1993**, *32*, 3844-3850.

[36] A. D. Hugi, L. Helm, A. E. Merbach, *Helv. Chim. Acta* **1985**, *68*, 508-521.

[37] F. Yerly, *VISUALISEUR 2.3.5 and OPTIMISEUR 2.3.5*, Lausanne, Switzerland, **1999**.

[38] a) T. J. Swift, R. E. Connick, *The Journal of Chemical Physics* **1962**, *37*, 307-320; b) K. Micskei, L. Helm, E. Brucher, A. E. Merbach, *Inorg. Chem.* **1993**, *32*, 3844-3850; c) H. G. Brittain, J. F. Desreux, *Inorg. Chem.* **1984**, *23*, 4459-4466; d) Z. Luz, S. Meibomm, *J.Am.Chem.Soc.* **1964**, *86*, 4766-4768; e) J. H. Freed, *J.Chem.Phys.* **1978**, *68*, 4034-4037; f) S. H. Koenig, R. D. Brown, *Prog. Nucl. Magn. Reson. Spectrosc.* **1990**, *22*, 487-567.

Entry for the Table of Contents

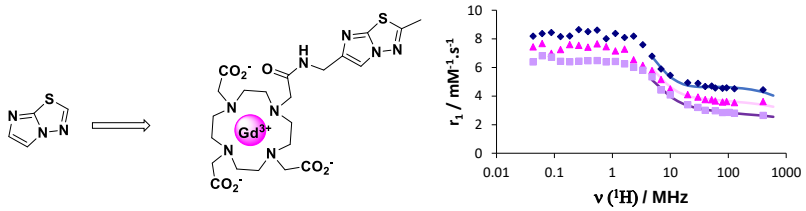

Efficient routes to the synthesis of DO3A-imidazo[2,1-b][1,3,4]thiadiazole complexes from readily accessible starting materials were investigated. The photophysical properties of the Tb^{3+} complexes have been determined. The corresponding Gd^{3+} complexes were also investigated and show a higher relaxivity than GdDOTA, without any aggregation process.

Electronic Supplementary Information

Synthesis, Luminescence and Relaxometric Properties of Macrocyclic Lanthanide Complexes Appended with an Imidazothiadiazole, a Heterocyclic Bioactive Scaffold

Modou Ndiaye, Emma Caillet, Svetlana V. Eliseeva, Thibaut Masson, Luke A. Marchetti, Agnès Pallier, Jean-François Morfin, Stéphane Petoud, Sylvain Routier, Frédéric Buron,* and Célia S. Bonnet*

Table of contents

Synthesis :

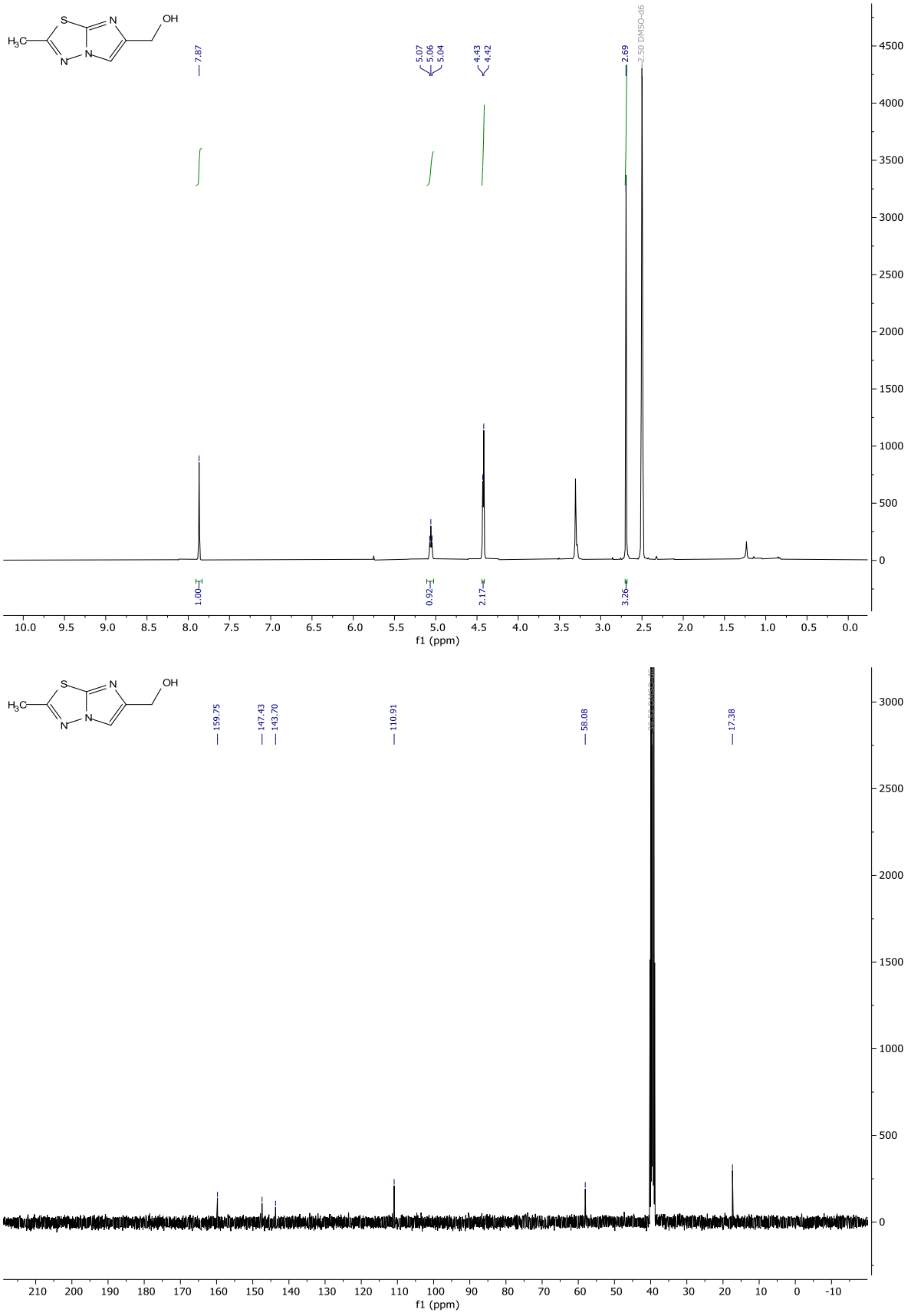

Figure S1 : ^{1}H and ^{13}C NMR spectra of compound **3.**

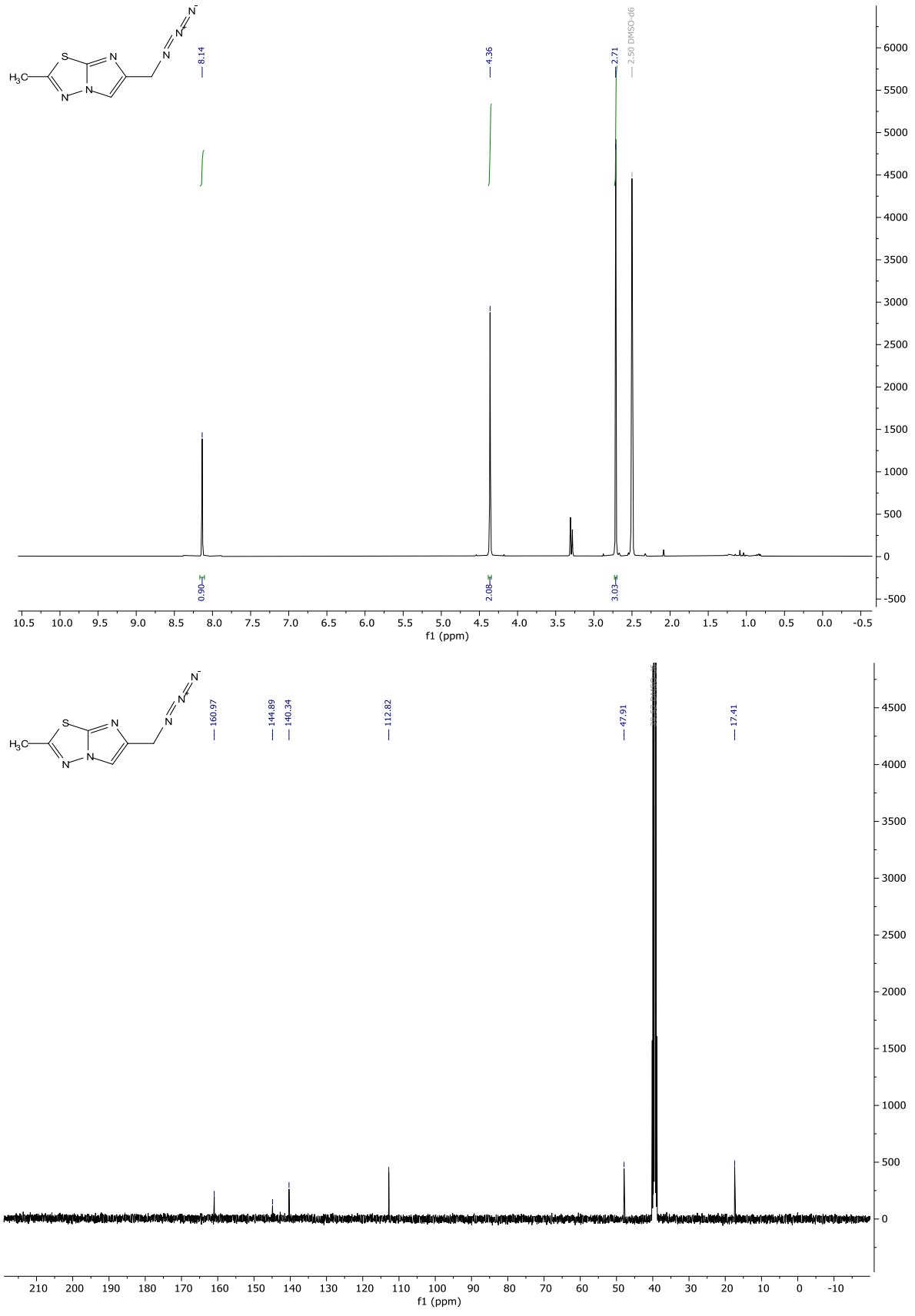

Figure S2 : ^{1}H and ^{13}C NMR spectra of compound **4.**

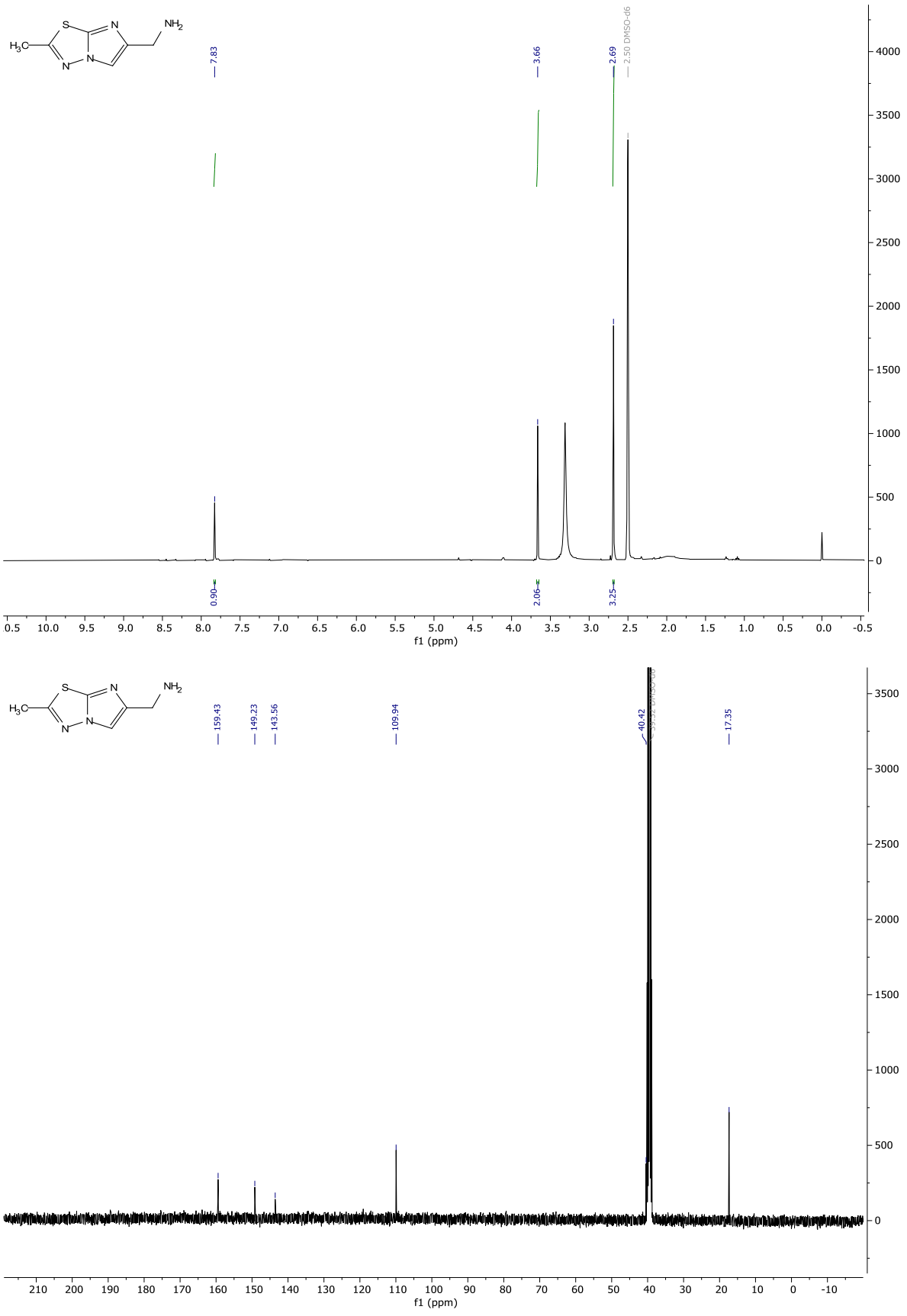

Figure S3 : ^{1}H and ^{13}C NMR spectra of compound **5.**

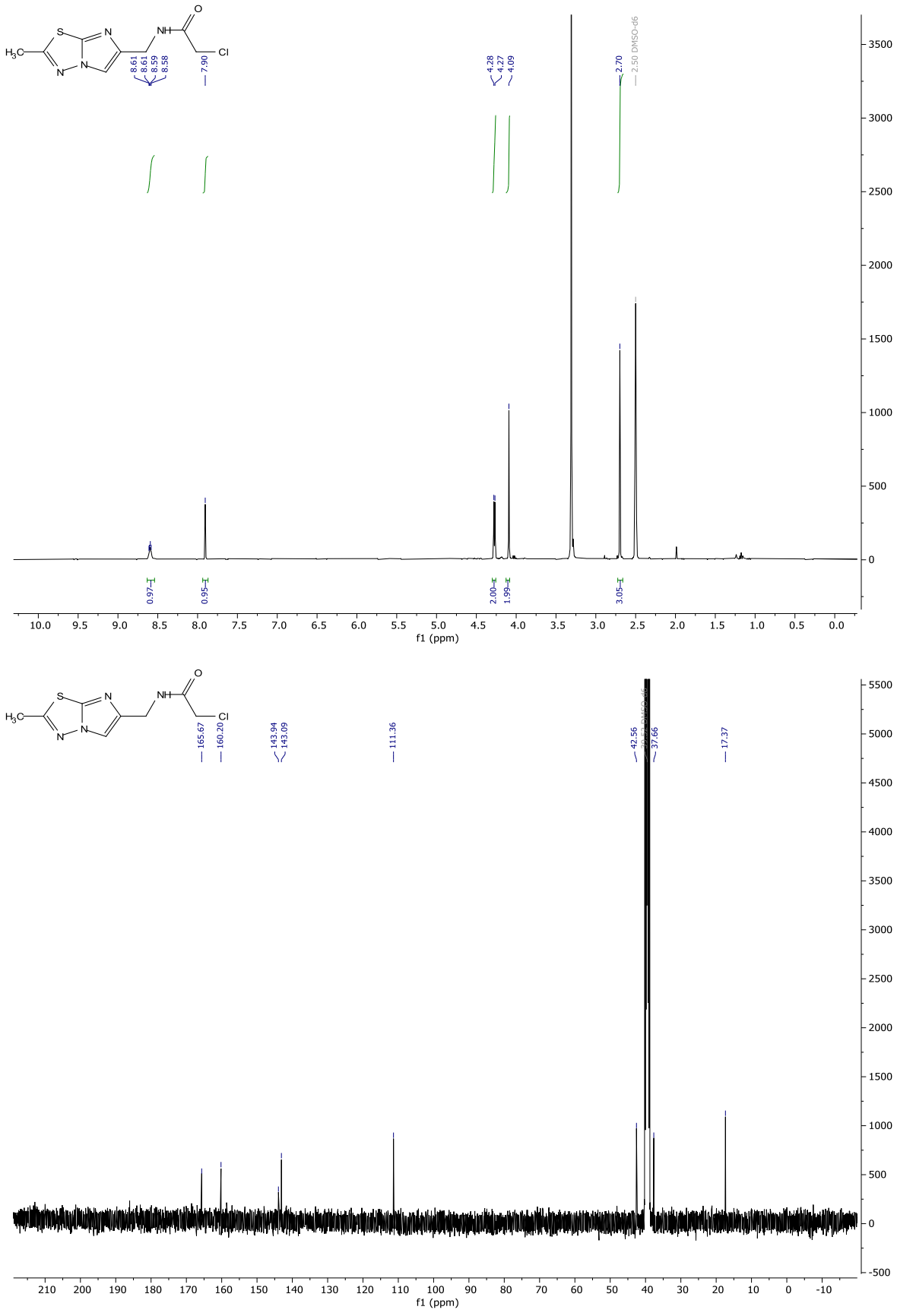

Figure S4 : ^{1}H and ^{13}C NMR spectra of compound **6.**

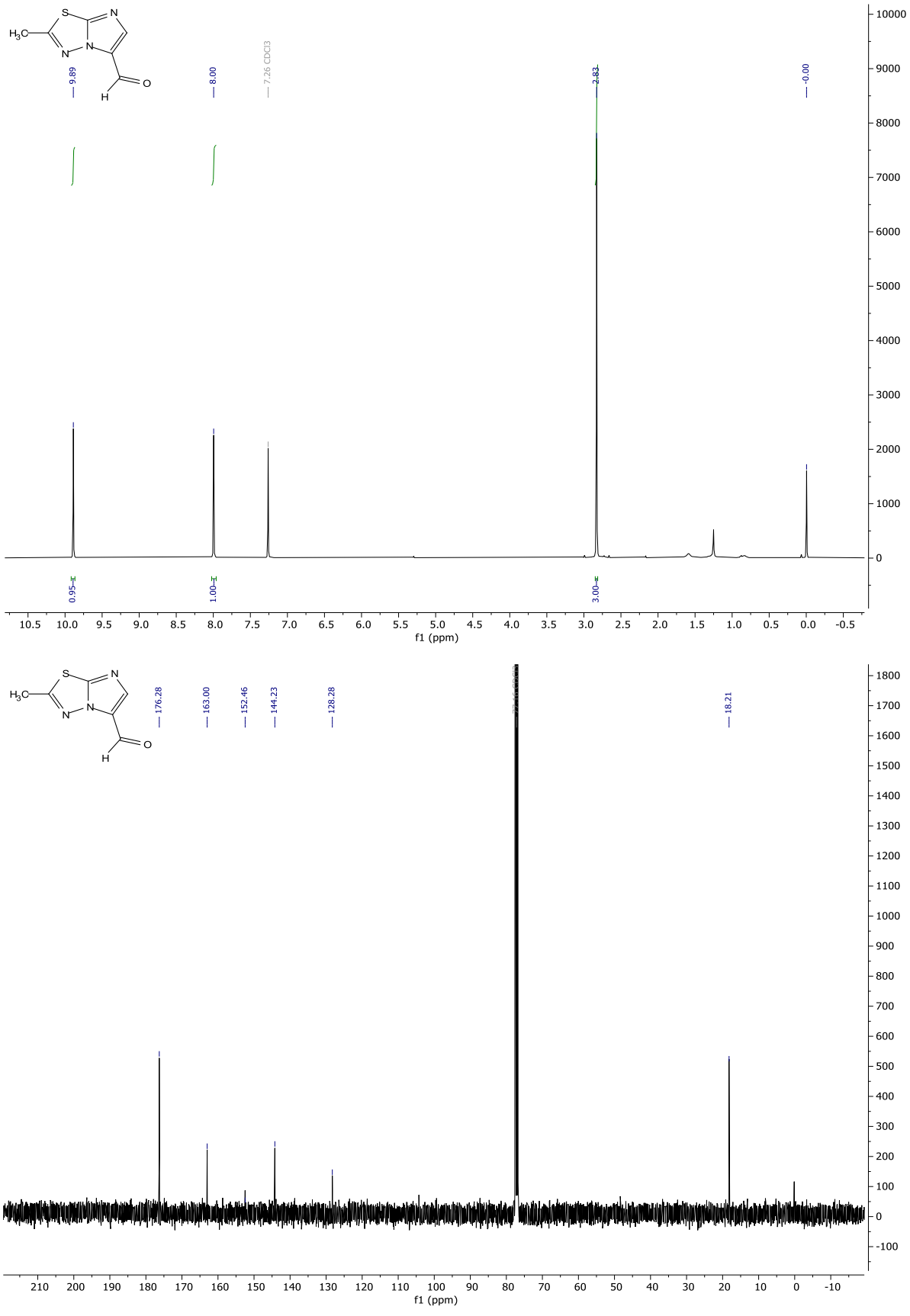

Figure S5 : ^{1}H and ^{13}C NMR spectra of compound **8.**

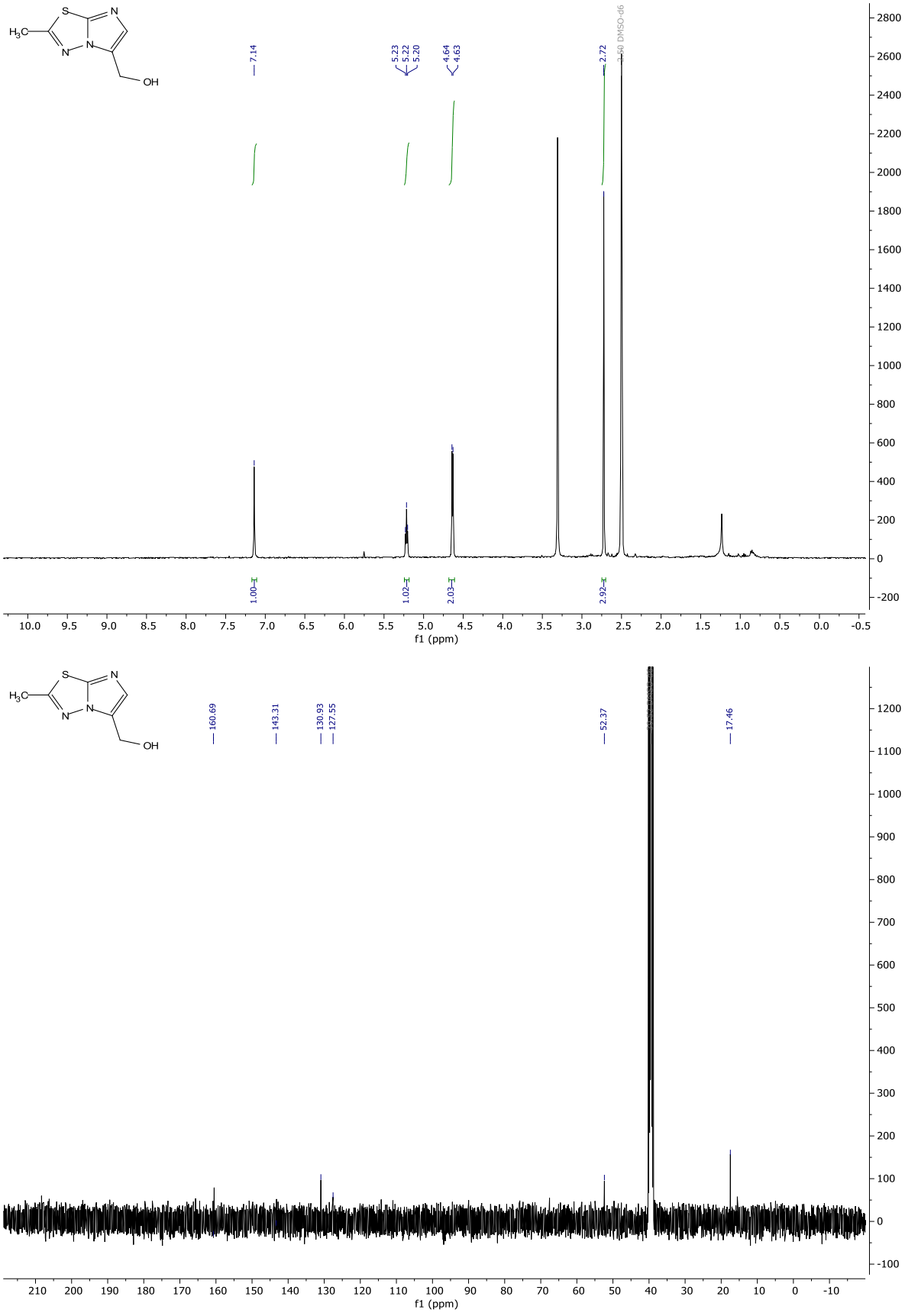

Figure S6: ^{1}H and ^{13}C NMR spectra of compound **9.**

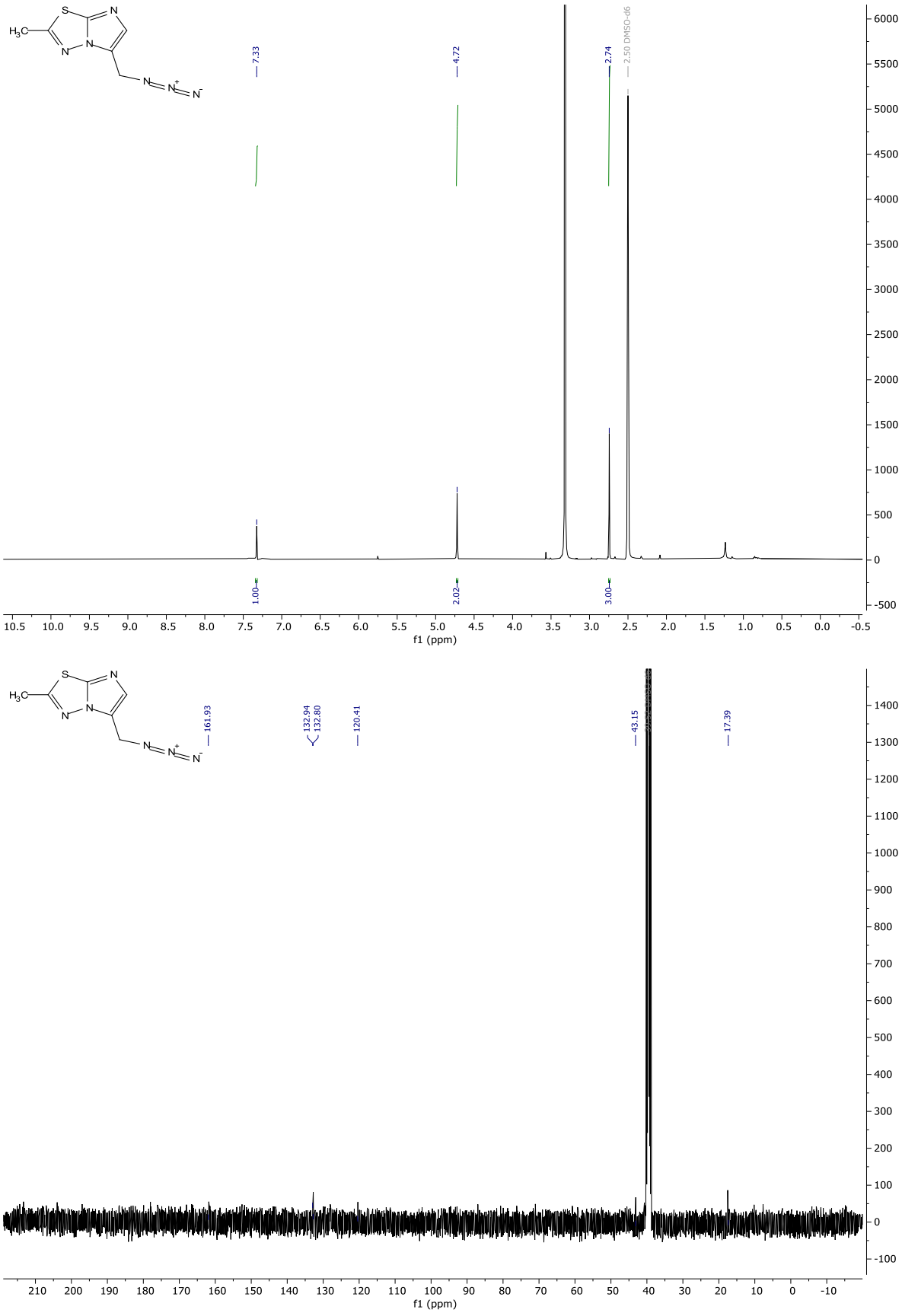

Figure S7 : ^{1}H and ^{13}C NMR spectra of compound **10.**

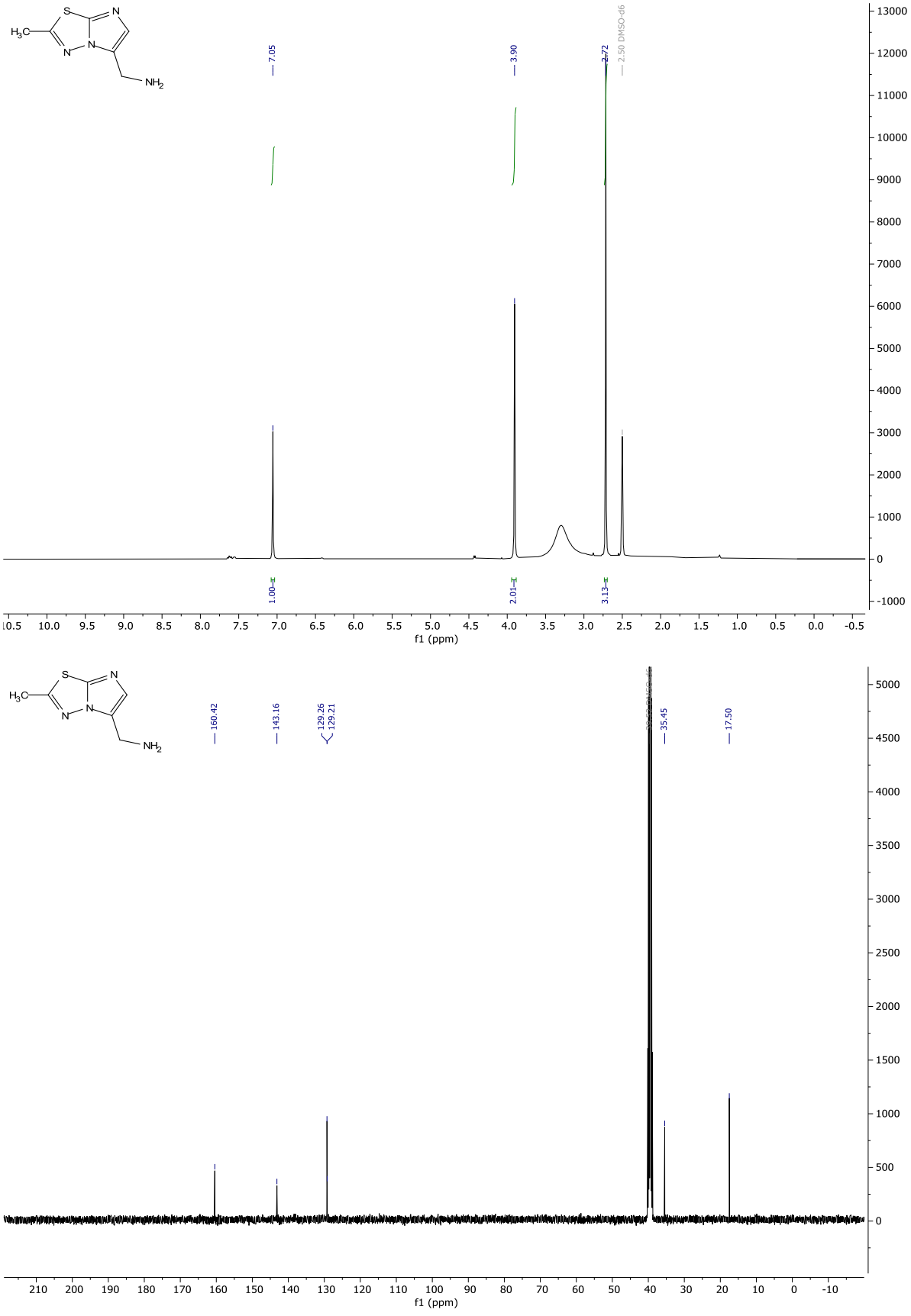

Figure S8 : ^{1}H and ^{13}C NMR spectra of compound **11.**

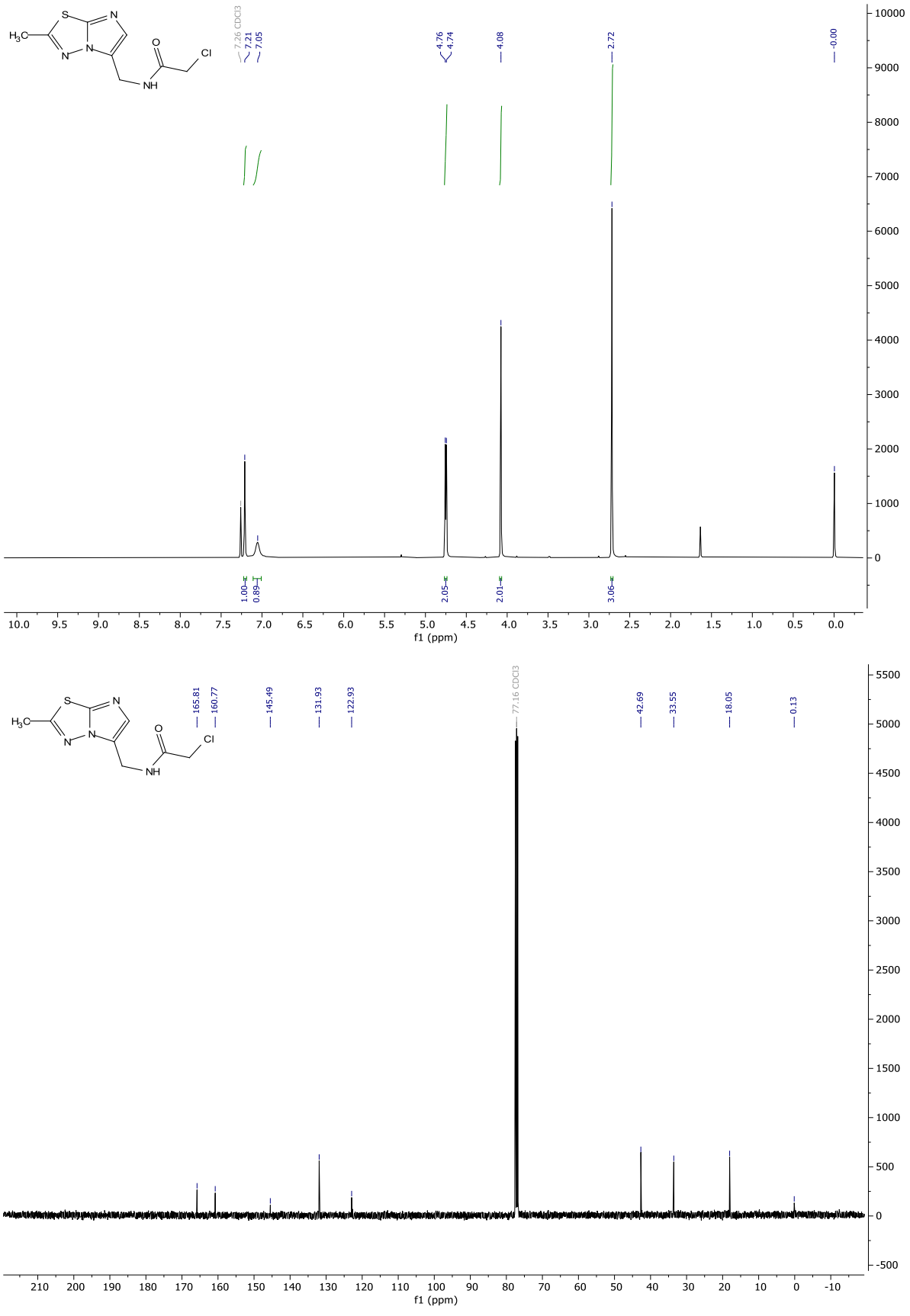

Figure S9 : ^{1}H and ^{13}C NMR spectra of compound **12.**

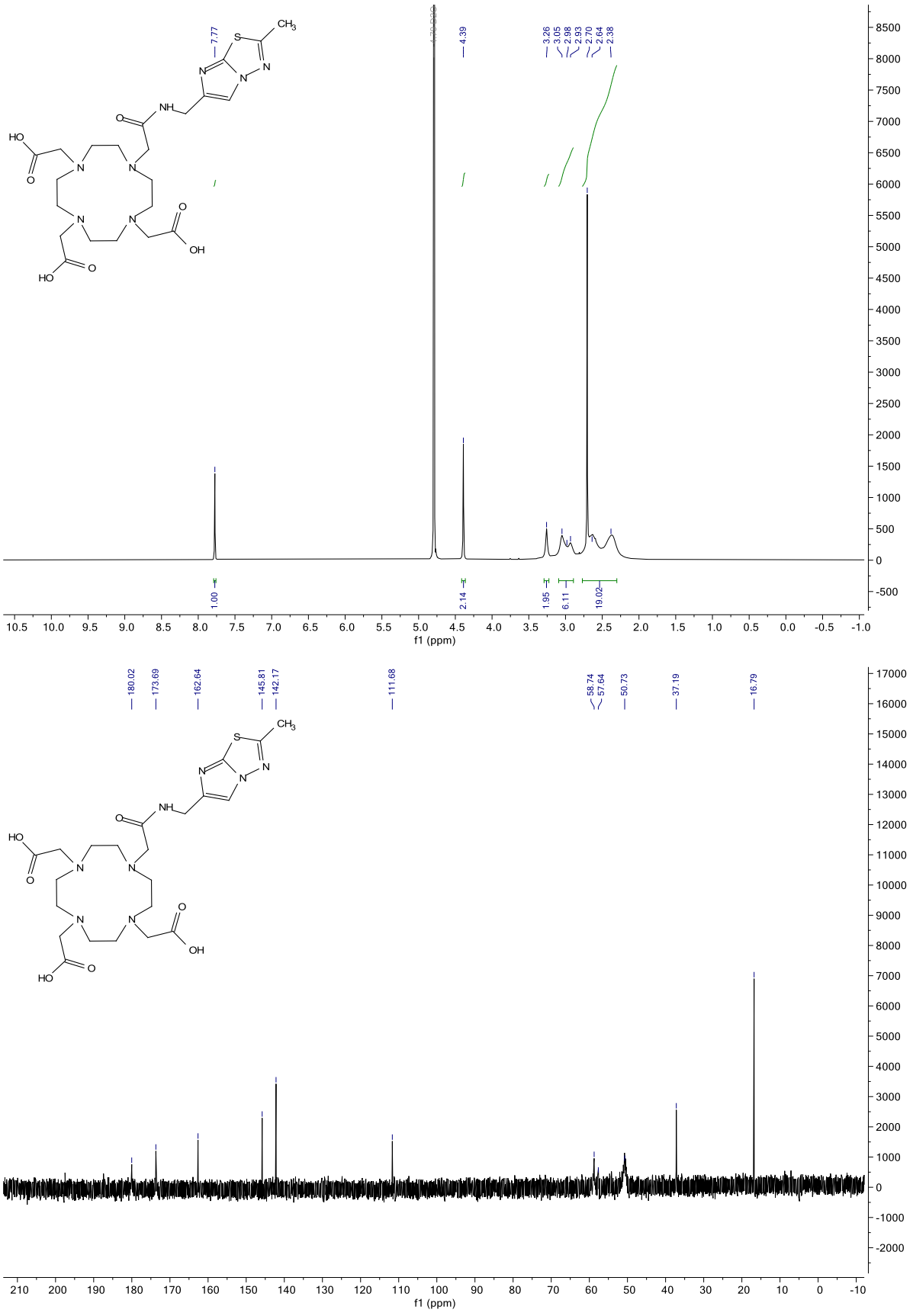

Figure S10 : ^{1}H and ^{13}C NMR spectra of compound **L1.**

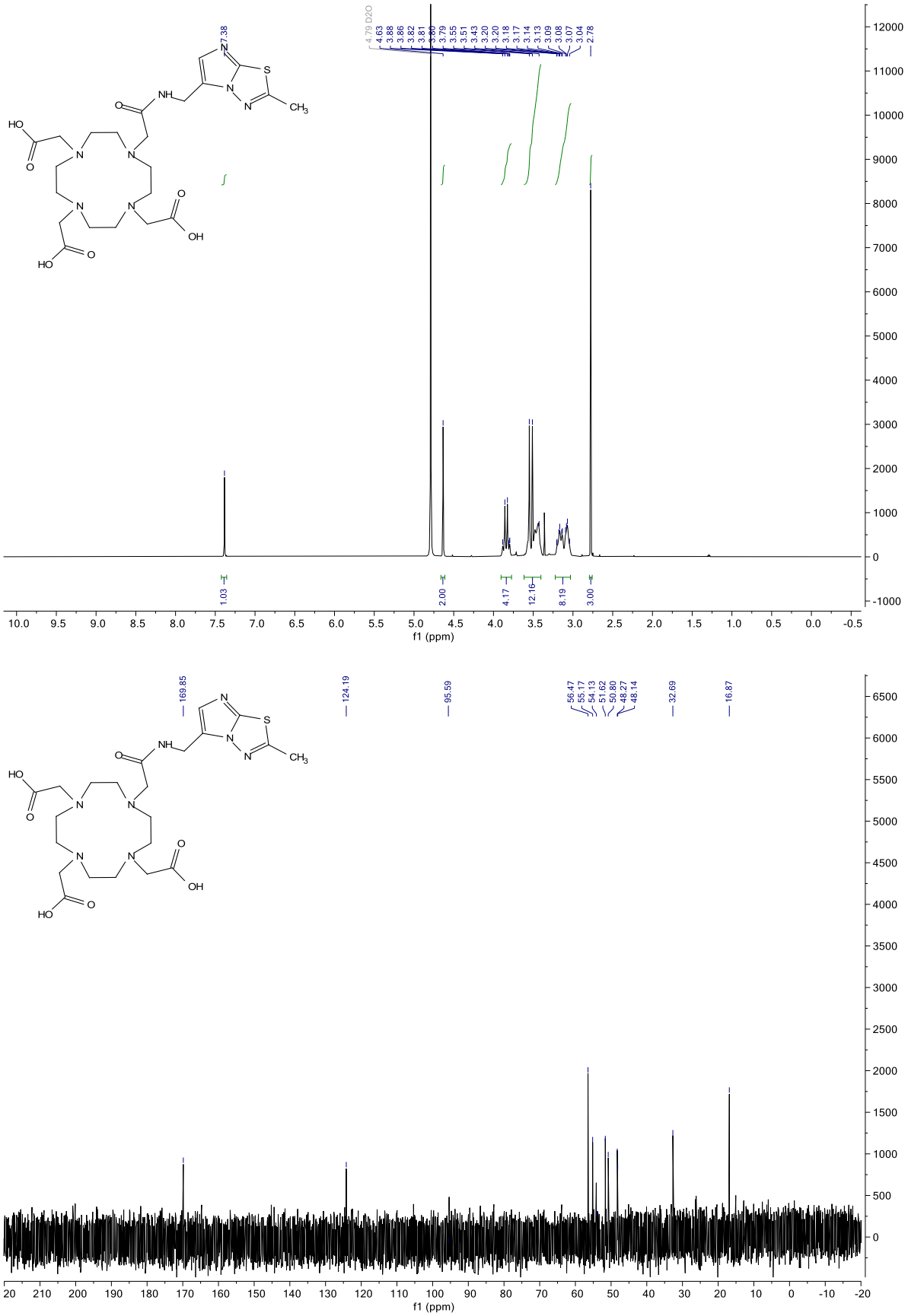

Figure S11 : ^{1}H and ^{13}C NMR spectra of compound **L2.**

Photophysical measurements :

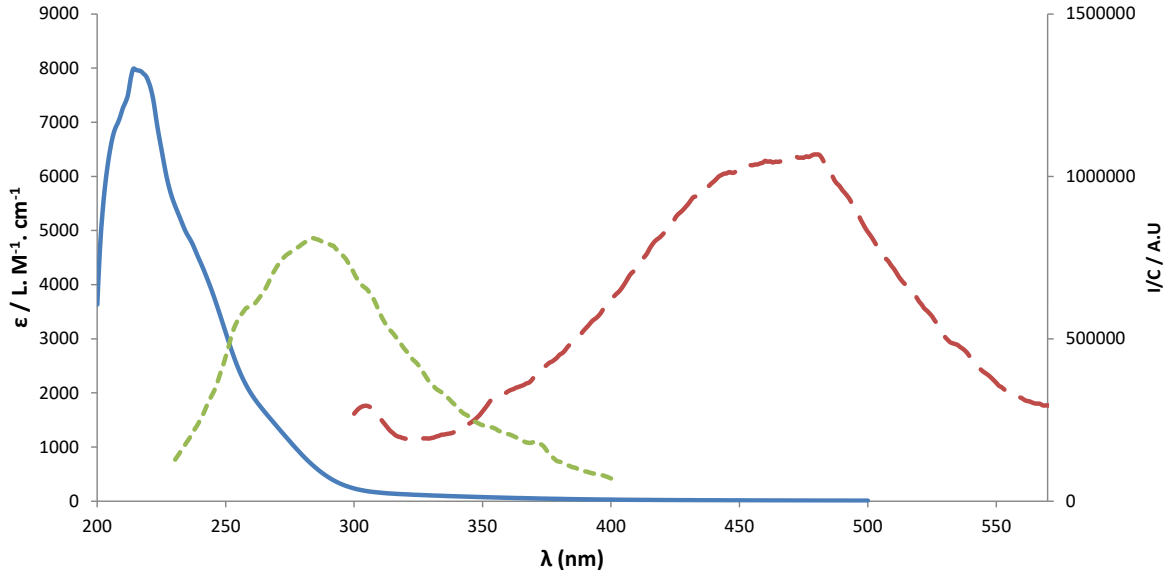

Figure S12. Absorption, emission (λ_{exc} = 270 nm), and excitation (λ_{em} = 400 nm) spectra of L1 (0.47 mM), pH 7.38, in NaCl 0.1 M.

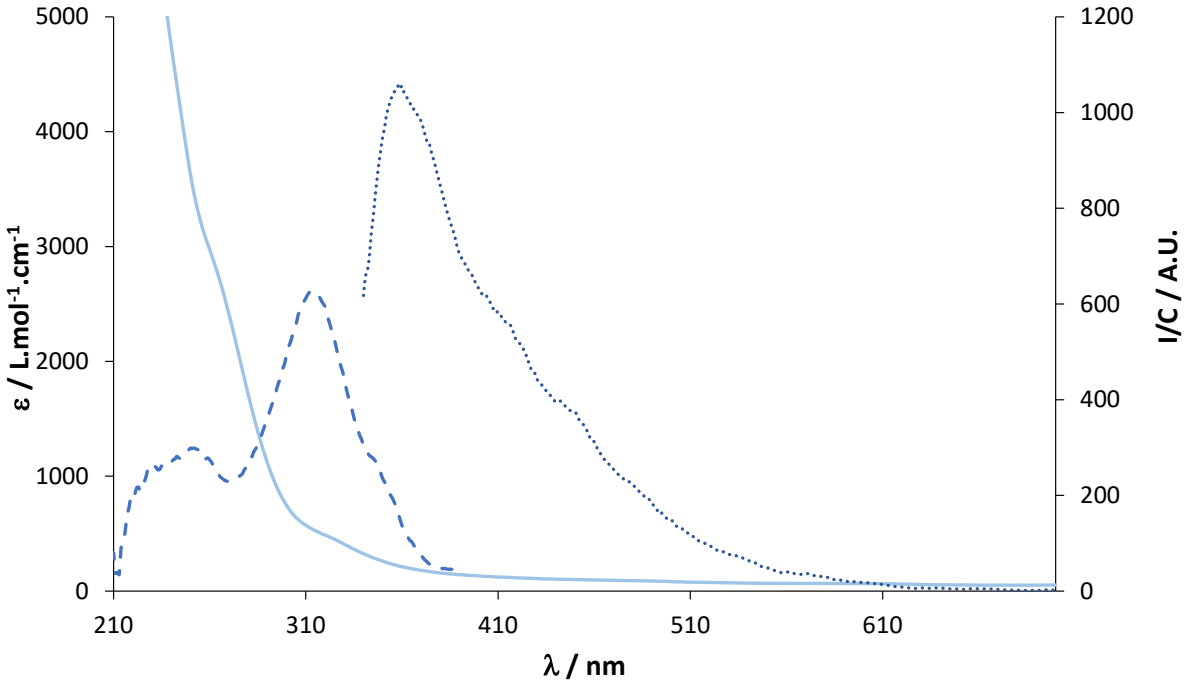

Figure S13. Absorption, emission (λ_{exc} = 315 nm), and excitation (λ_{em} = 363 nm) spectra of L2 (0.2 mM), pH 7.8, in NaCl 0.1 M.

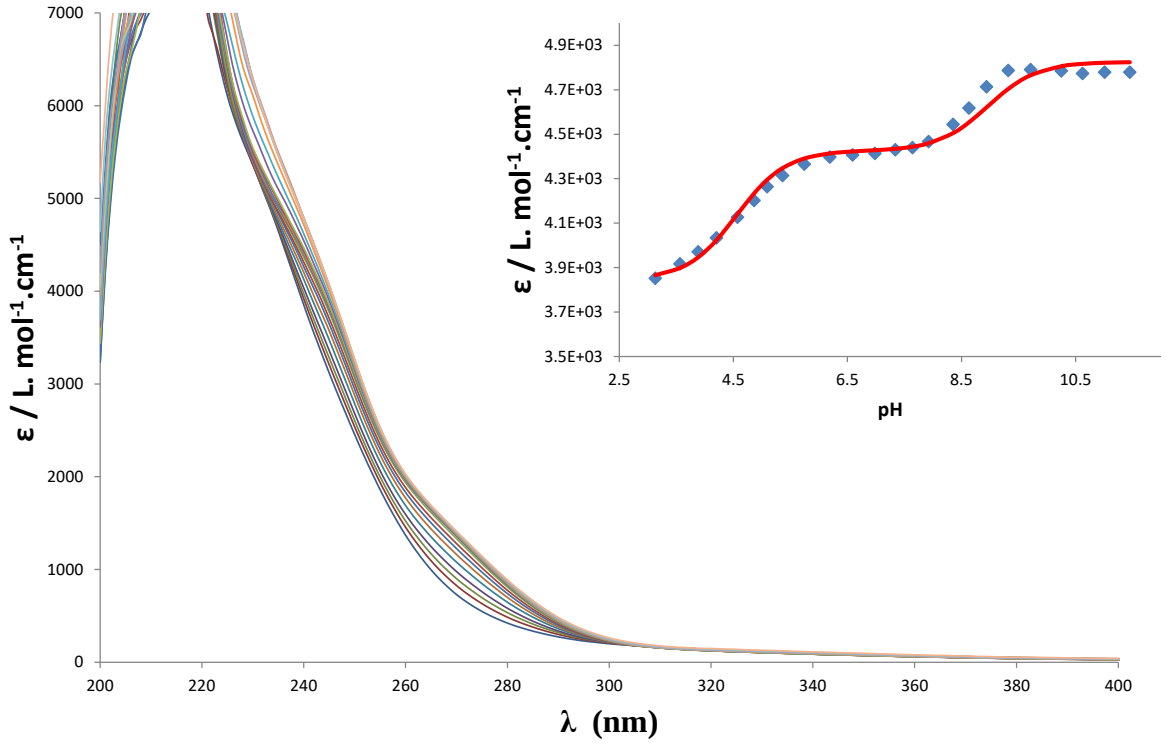

Figure S14. Absorption spectra of L1 (0.47 mM) in NaCl 0.1 M at 25°C ; inset : molar absoprtion coefficients at 240 nm as a function of pH (The diamonds represent experimentally obtained data points while the solid line respresents the fitted data).

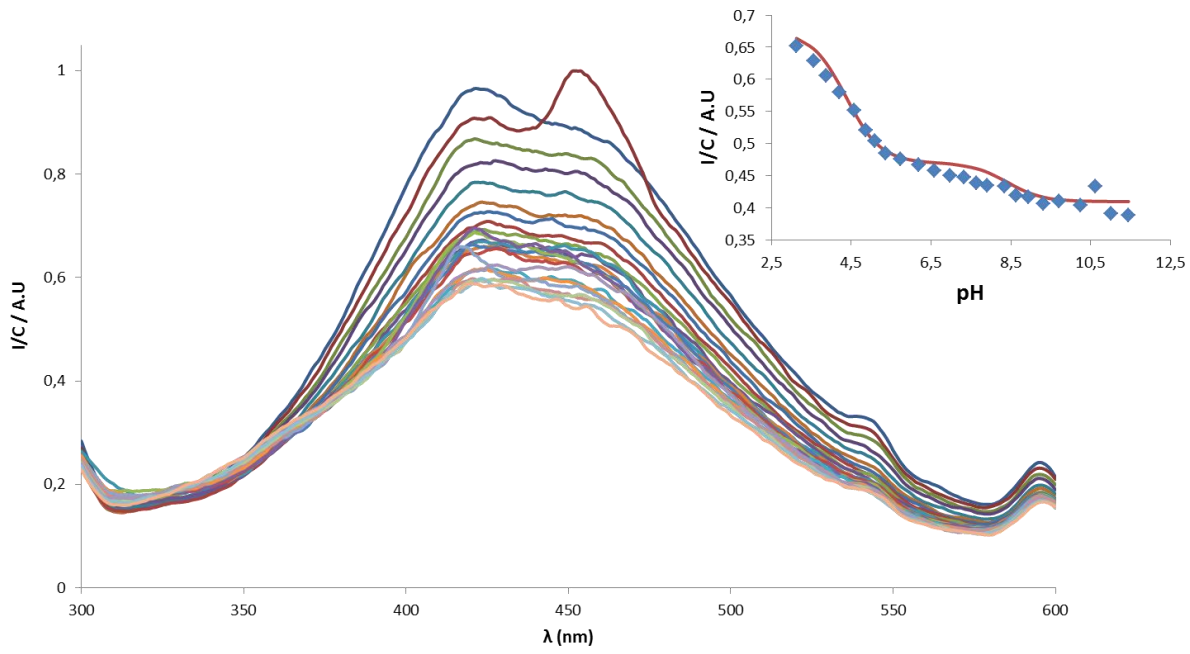

Figure S15. Normalized emission spectra (λ_{exc} = 270 nm) of L1 (0.47 mM) in NaCl 0.1 M at 25°C ; Inset: Intensity as a function of pH at 490 nm. The line represents the best fit obtained with the parameters form Table 1.

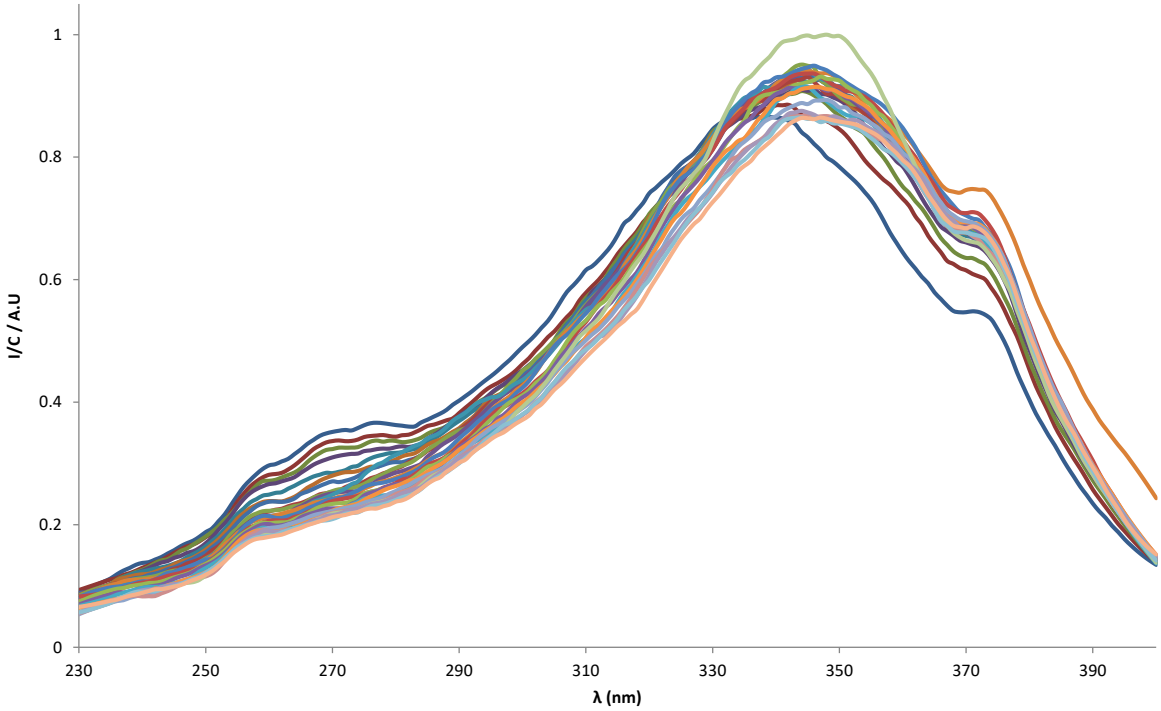

Figure S16. Normalized excitation spectra of L1 (0.47 mM) in NaCl 0.1 M as a function of pH (λ_{em} = 400 nm) at 25°C .

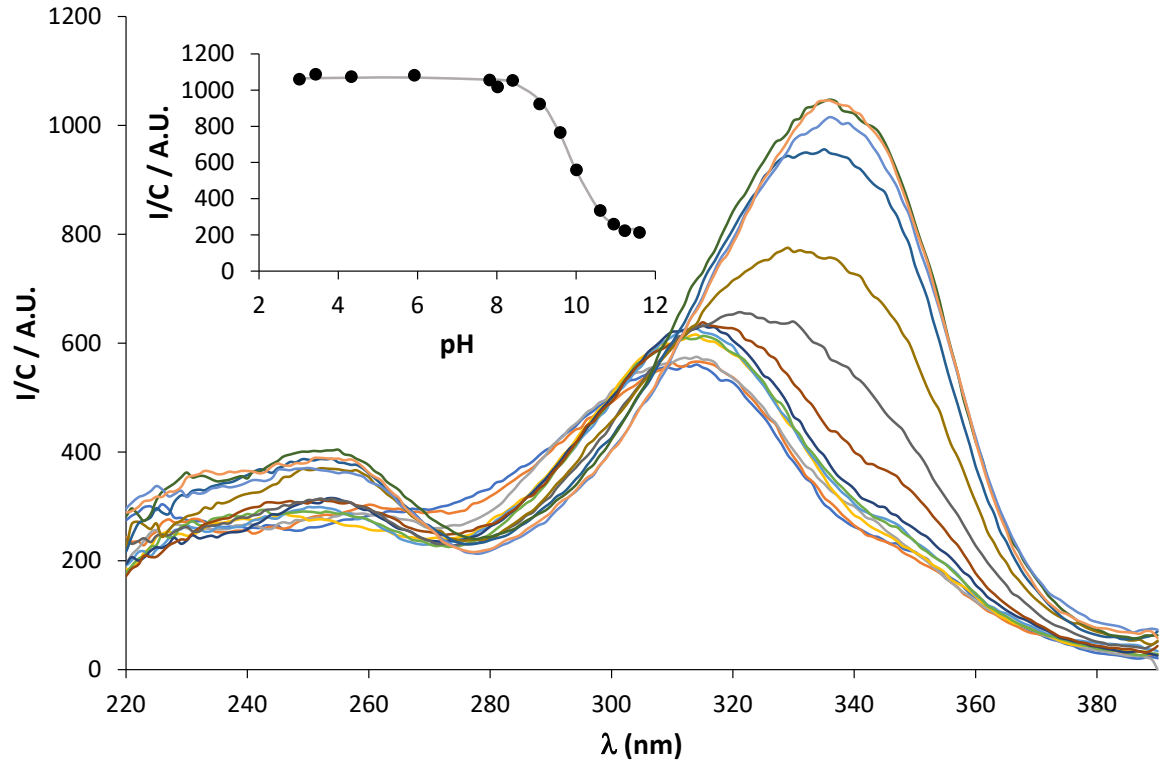

Figure S17. Excitation spectra of L2 (0.2 mM) in NaCl 0.1 M (λ_{em} = 400 nm) at 25°C ; inset : normalized emission intensities at 336 nm as a function of pH (the line represents the best fit with the values presented in Table 1).

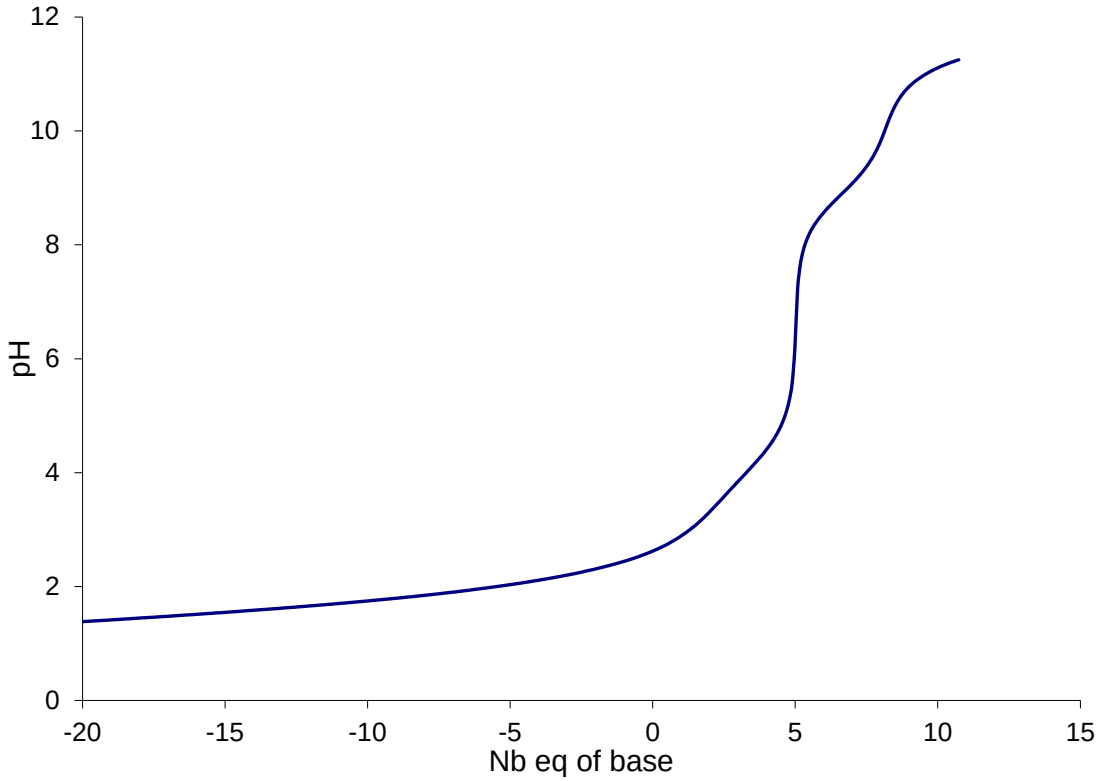

Figure S18. Potentiometric titrations of L2 (3.47 mM) in NaCl 0.15 M at 25°C

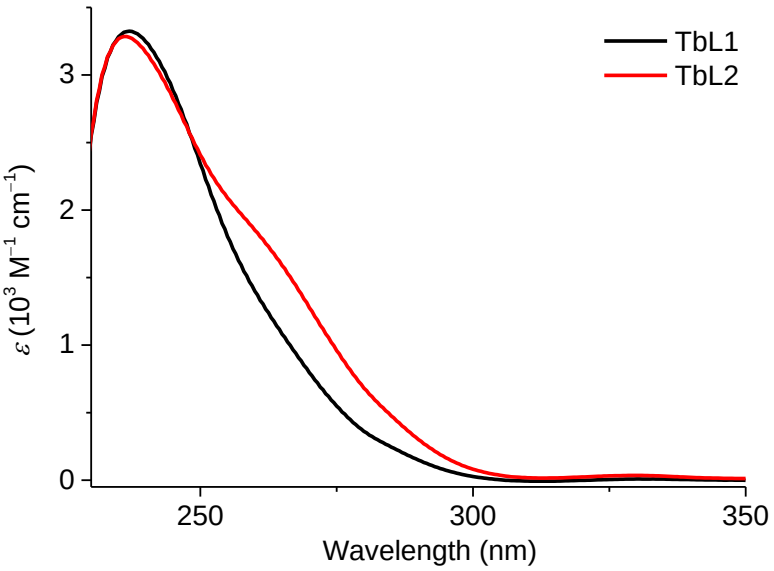

Figure S19. Absorption spectra of Tb^{3+} complexes (0.5 mM, HEPES pH 7.4, room temperature).

Table S1. Tb^{3+}-centered luminescence lifetimes.[a]

Compound	Solvent	τ_{obs} (ms)[b]
TbL1	HEPES, pH 7.4	1.4(1): 91(3)% 0.32(2): 9(3)% τ_{av} = 1.3(1)
	D_2O, pD = 7.4	1.4(1): 86(3)% 0.67(2): 14(3)% τ_{av} = 1.3(1)
TbL2	HEPES, pH 7.4	1.6(1): 92(3)% 0.34(2): 8(3)% τ_{av} = 1.5(1)
	D_2O, pD = 7.4	2.1(1): 85(2)% 0.67(2): 15(2)% τ_{av} = 1.9(1)

[a] For 0.5 mM solutions at room temperature; 2σ values are given between parentheses. Experimental errors: τ_{obs}, ±5%. [b] Under excitation at 266 nm.

Relaxivity data:

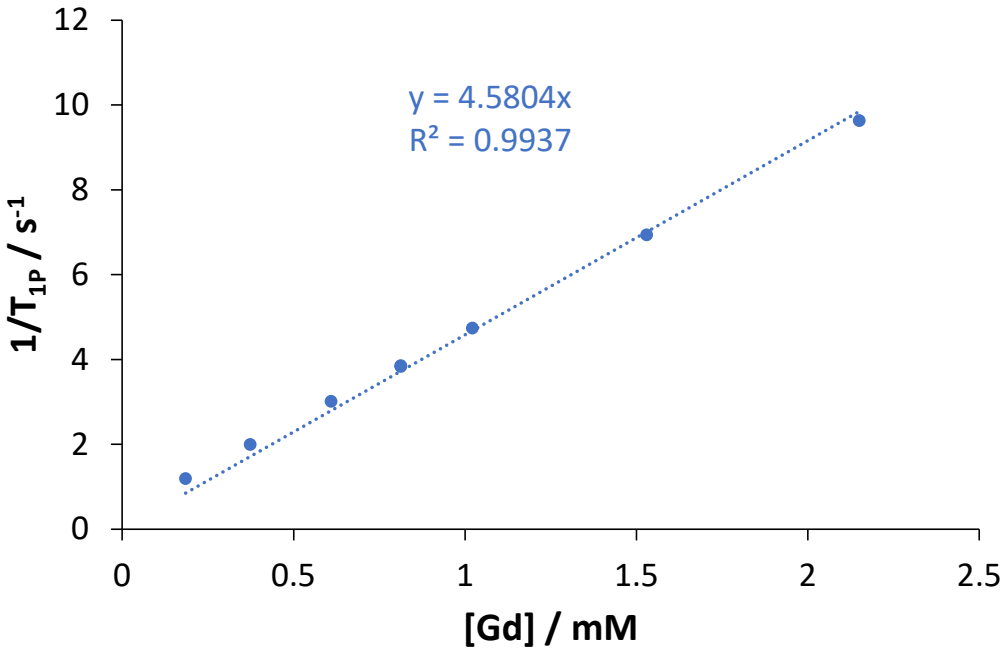

Figure S20. Paramagnetic Relaxation Enhancement measurements in the presence of GdL1 at 60 MHz, 25°C.

Table S2. Parameters obtained from the simultaneous fitting of the transverse ^{17}O NMR relaxation rates and chemical shifts as a function of temperature at 9.4 T, and of the NMRD profiles at 298 K, 310 K, and 323 K, using the Solomon Bloembergen and Morgan theory presented below.

	GdL1	**GdL2**
k_{ex}^{298} ($10^6 s^{-1}$)	2.2 (2)	2.0 (1)
$\Delta H^{\neq}$ ($kJ.mol^{-1}$)	49 (3)	49 (2)
τ_R^{298} (ps)[a],[b]	98 (2)	92 (2)
E_R ($kJ.mol^{-1}$)	17 (2)	18 (2)
τ_v^{298} (ps)	8.3 (7)	7.1 (5)
Δ^2 ($10^{20} s^{-1}$)	0.84 (6)	0.77 (5)
A/ħ ($10^6 rad.s^{-1}$)	-3.8 (2)	-3.6 (2)
D_{GdH}^{298} (10^{-9} $m^2 s^{-1}$)[a]	26	26
E_{DGdH} ($kJ.mol^{-1}$)	22 (3)	20 (2)
C_{os}	0.23 (7)	0.16 (4)

Equations used for the analysis of the ^{17}O NMR and NMRD data

^{17}O NMR spectroscopy

From the measured ^{17}O NMR relaxation rates and angular frequencies of the paramagnetic solutions, $1/T_2$, $1/T_1$ and ω, and from the acidified water reference, $1/T_{2A}$, $1/T_{1A}$ and ω_A, it is possible to calculate the reduced relaxation rates and chemical shifts, $1/T_{2r}$, $1/T_{1r}$ and $\Delta\omega_r$ (Eq. 1-3), where $1/T_{1m}$ and $1/T_{2m}$ are the relaxation rate of the bound water and $\Delta\omega_m$ is the chemical shift difference between bound and bulk water, τ_m is the mean residence time or the inverse of the water exchange rate k_{ex} and P_m is the mole fraction of the bound water.[1]

$$\frac{1}{T_{1r}} = \frac{1}{P_m}\left[\frac{1}{T_1} - \frac{1}{T_{1A}}\right] = \frac{1}{T_{1m} + \tau_m} + \frac{1}{T_{1os}} \qquad [1]$$

$$\frac{1}{T_{2r}} = \frac{1}{P_m}\left[\frac{1}{T_2} - \frac{1}{T_{2A}}\right] = \frac{1}{\tau_m}\frac{T_{2m}^{-2} + \tau_m^{-1}T_{2m}^{-1} + \Delta\omega_m^2}{(\tau_m^{-1} + T_{2m}^{-1})^2 + \Delta\omega_m^2} + \frac{1}{T_{2os}} \qquad [2]$$

$$\Delta\omega_r = \frac{1}{P_m}(\omega - \omega_A) = \frac{\Delta\omega_m}{(1 + \tau_m T_{2m}^{-1})^2 + \tau_m^2\Delta\omega_m^2} + \Delta\omega_{os} \qquad [3]$$

The outer sphere contributions to the ^{17}O relaxation rates $1/T_{1OS}$ and $1/T_{2OS}$ can be neglected according to previous studies.[2] Eqs. 1-2 can be further simplified into Eqs. 4-5:

$$\frac{1}{T_{1r}} = \frac{1}{T_{1m} + \tau_m} \qquad [4]$$

$$\frac{1}{T_{2r}} = \frac{1}{T_{2m} + \tau_m} \qquad [5]$$

The exchange rate is assumed to be described by the Eyring equation (Eq 6), where $\Delta S^{\ddagger}$ and $\Delta H^{\ddagger}$ are the entropy and enthalpy of activation for the water exchange process, and k_{ex}^{298} is the exchange rate at 298.15 K. R is the usual gas constant whereas h and k_B are the Planck and Boltzmann constants, respectively:

$$\frac{1}{\tau_m} = k_{ex} = \frac{k_B T}{h} exp\left\{\frac{\Delta S^{\ddagger}}{R} - \frac{\Delta H^{\ddagger}}{RT}\right\} = \frac{k_{ex}^{298} T}{298.15} exp\left\{\frac{\Delta H^{\ddagger}}{R}\left(\frac{1}{298.15} - \frac{1}{T}\right)\right\} \quad [6]$$

In the transverse relaxation the scalar contribution, $1/T_{2sc}$, is the most important. In Eq. 7 $1/\tau_{s1}$ is the sum of the exchange rate and the electron spin relaxation rate constants.

$$\frac{1}{T_{2m}} \cong \frac{1}{T_{2sc}} = \frac{S(S+1)}{3}\left(\frac{A}{\hbar}\right)^2 \left(\tau_{s1} + \frac{\tau_{s2}}{1+\omega_S^2 \tau_{s2}^2}\right) \quad [7]$$

$$\frac{1}{\tau_{s1}} = \frac{1}{\tau_m} + \frac{1}{T_{1e}} \quad [8]$$

The ^{17}O longitudinal relaxation rates in Gd^{3+} solutions are the sum of the contributions of the dipole-dipole (*dd*) and quadrupolar (*q*) mechanisms as expressed by Equations (11-13) for non-extreme narrowing conditions, where γ_S is the electron and γ_I is the nuclear gyromagnetic ratio (γ_S = 1.76×10^{11} rad s^{-1} T^{-1}, γ_I=-3.626×10^{7} rad s^{-1} T^{-1}), r_{GdO} is the effective distance between the electron charge and the ^{17}O nucleus, I is the nuclear spin (5/2 for ^{17}O), χ is the quadrupolar coupling constant and η is an asymmetry parameter :

$$\frac{1}{T_{1m}} = \frac{1}{T_{1dd}} + \frac{1}{T_{1q}} \quad [9]$$

with:

$$\frac{1}{T_{1dd}} = \frac{2}{15}\left(\frac{\mu_0}{4\pi}\right)^2 \frac{\hbar^2\gamma_I^2\gamma_S^2}{r_{GdO}^6} S(S+1)\times\left[3J(\omega_I;\tau_{d1})+7J(\omega_S;\tau_{d2})\right] \quad [10]$$

$$\frac{1}{T_{1q}} = \frac{3\pi^2}{10}\frac{2I+3}{I^2(2I-1)}\chi^2(1+\eta^2/3)\times\left[0.2J_1(\omega_I)+0.8J_2(\omega_I)\right] \quad [11]$$

In Eq. 3, the chemical shift of the bound water molecule, $\Delta\omega_m$, depends on the hyperfine interaction between the Gd^{3+} electron spin and the ^{17}O nucleus and is directly proportional to the scalar coupling constant, $A/\hbar$, as expressed in Eq. 7.[3]

$$\Delta\omega_m = \frac{g_L\mu_B S(S+1)B}{3k_BT}\frac{A}{\hbar} \quad [12]$$

The isotopic Landé g factor is equal to 2.0 for the Gd^{3+}, B represents the magnetic field, and k_B is the Boltzmann constant.

^{1}H NMRD

The measured longitudinal proton relaxation rate, R_1^{obs} is the sum of the paramagnetic and diamagnetic contributions as expressed in Eq. 13, where r_1 is the proton relaxivity:

$$R_1^{obs} = R_1^d + R_1^p = R_1^d + r_1\times c_{Gd} \quad [13]$$

The relaxivity can be divided into terms of inner and outer sphere, as follows:

$$r_1 = r_{1is} + r_{1os} \quad [14]$$

The inner sphere term is obtained in Eq. 15, where *q* is the number of inner sphere water molecules.[4]

$$r_{1is} = \frac{1}{1000} \times \frac{q}{55.55} \times \frac{1}{T_{1m}^{H} + \tau_m} \qquad [15]$$

The longitudinal relaxation rate of inner sphere protons, $1/T_{1m}^{H}$ is expressed by Eq. 16, where r_{GdH} is the effective distance between the electron charge and the ^{1}H nucleus, ω_I is the proton resonance frequency and ω_S is the Larmor frequency of the Gd^{III} electron spin.

$$\frac{1}{T_{1m}^{H}} = \frac{2}{15}\left(\frac{\mu_0}{4\pi}\right)^2 \frac{\hbar^2 \gamma_I^2 \gamma_S^2}{r_{GdH}^6} S(S+1) \times \left[3J(\omega_I ; \tau_{d1}) + 7J(\omega_S ; \tau_{d2})\right] \qquad [16]$$

$$\frac{1}{\tau_{di}} = \frac{1}{\tau_m} + \frac{1}{\tau} + \frac{1}{T_{ie}} \qquad [17]$$

The longitudinal and transverse electronic relaxation rates, $1/T_{1e}$ and $1/T_{2e}$ are expressed by Eq. 18-19, where τ_V is the electronic correlation time for the modulation of the zero-field-splitting interaction, E_V the corresponding activation energy and Δ^2 is the mean square zero-field-splitting energy. We assumed a simple exponential dependence of τ_V versus $1/T$.

$$\left(\frac{1}{T_{1e}}\right)^{ZFS} = \frac{1}{25}\Delta^2 \tau_v \{4S(S+1) - 3\}\left(\frac{1}{1+\omega_S^2 \tau_v^2} + \frac{4}{1+4\omega_S^2 \tau_v^2}\right) \qquad [18]$$

$$\left(\frac{1}{T_{2e}}\right)^{ZFS} = \Delta^2 \tau_v \left(\frac{5.26}{1+0.372\omega_S^2 \tau_v^2} + \frac{7.18}{1+1.24\omega_S \tau_v}\right) \qquad [19]$$

$$\tau_v = \tau_v^{298} exp\left\{\frac{E_v}{R}\left(\frac{1}{T} - \frac{1}{298.15}\right)\right\} \qquad [20]$$

The outer-sphere contribution can be described by Eq. 17 where N_A is the Avogadro constant, and J_{os} is its associated spectral density function.[5],[6]

$$r_{1os} = \frac{32N_A\pi}{405}\left(\frac{\mu_0}{4\pi}\right)^2 \frac{\hbar^2\gamma_S^2\gamma_I^2}{a_{GdH}D_{GdH}} S(S+1)\left[3J_{os}(\omega_I, T_{1e}) + 7J_{os}(\omega_S, T_{2e})\right] \qquad [21]$$

$$J_{os}(\omega, T_{je}) = Re\left[\frac{1 + \frac{1}{4}\left(i\omega\tau_{GdH} + \frac{\tau_{GdH}}{T_{je}}\right)^{1/2}}{1 + \left(i\omega\tau_{GdH} + \frac{\tau_{GdH}}{T_{je}}\right)^{1/2} + \frac{4}{9}\left(i\omega\tau_{GdH} + \frac{\tau_{GdH}}{T_{je}}\right) + \frac{1}{9}\left(i\omega\tau_{GdH} + \frac{\tau_{GdH}}{T_{je}}\right)^{3/2}}\right] \qquad j = 1, 2 \qquad [22]$$

The diffusion coefficient for the diffusion of a water proton away from a Gd^{III} complex, D_{GdH}, is assumed to obey an exponential law versus the inverse of the temperature, with an activation energy $E_{GdH,}$ as given in Eq. 23 D_{GdH}^{298} is the diffusion coefficient at 298.15 K.

$$D_{\mathrm{GdH}} = D_{\mathrm{GdH}}^{298} \exp\left\{\frac{E_{\mathrm{GdH}}}{R}\left(\frac{1}{298.15} - \frac{1}{T}\right)\right\} \qquad [23]$$

[1] T. J. Swift, R. E. Connick, *J. Chem. Phys.* **1962**, *37*, 307-&.
[2] K. Micskei, L. Helm, E. Brucher, A. E. Merbach, *Inorg. Chem.* **1993**, *32*, 3844-3850.
[3] H. G. Brittain, J. F. Desreux, *Inorg. Chem.* **1984**, *23*, 4459-4466.
[4] Z. Luz, S. Meiboom, *J. Chem. Phys.* **1964**, *40*, 2686-&.
[5] J. H. Freed, *J. Chem. Phys.* **1978**, *68*, 4034-4037.
[6] S. H. Koenig, R. D. Brown Iii, *Prog. Nucl. Magn. Reson. Spectrosc.* **1990**, *22*, 487-567.